

Review

# A Review of the Synthesis of Biopolymer Hydrogel Electrolytes for Improved Electrode–Electrolyte Interfaces in Zinc-Ion Batteries

Veerle Vandeginste \*  and Junru Wang

KU Leuven, Campus Bruges, Department of Materials Engineering, Surface and Interface Engineered Materials, 8200 Bruges, Belgium; junru.wang@kuleuven.be

\* Correspondence: veerle.vandeginste@kuleuven.be

**Abstract:** The market for electric vehicles and portable and wearable electronics is expanding rapidly. Lithium-ion batteries currently dominate the market, but concerns persist regarding cost and safety. Consequently, alternative battery chemistries are investigated, with zinc-ion batteries (ZIBs) emerging as promising candidates due to their favorable characteristics, including safety, cost-effectiveness, theoretical volumetric capacity, energy density, and ease of manufacturing. Hydrogel electrolytes stand out as advantageous for ZIBs compared to aqueous electrolytes. This is attributed to their potential application in flexible batteries for wearables and their beneficial impact in suppressing water-induced side reactions, zinc dendrite formation, electrode dissolution, and the risk of water leakage. The novelty of this review lies in highlighting the advancements in the design and synthesis of biopolymer hydrogel electrolytes in ZIBs over the past six years. Notable biopolymers include cellulose, carboxymethyl cellulose, chitosan, alginate, gelatin, agar, and gum. Also, double-network and triple-network hydrogel electrolytes have been developed where biopolymers were combined with synthetic polymers, in particular, polyacrylamide. Research efforts have primarily focused on enhancing the mechanical properties and ionic conductivity of hydrogel electrolytes. Additionally, there is a concerted emphasis on improving the electrochemical performance of semi-solid-state ZIBs. Moreover, some studies have delved into self-healing and adhesive properties, anti-freezing characteristics, and the multifunctionality of hydrogels. This review paper concludes with perspectives on potential future research directions.

**Keywords:** interfacial contact; interphase; quasi-solid-state; aqueous zinc-ion batteries



**Citation:** Vandeginste, V.; Wang, J. A Review of the Synthesis of Biopolymer Hydrogel Electrolytes for Improved Electrode–Electrolyte Interfaces in Zinc-Ion Batteries. *Energies* **2024**, *17*, 310. <https://doi.org/10.3390/en17020310>

Academic Editor: Antonino S. Aricò

Received: 25 November 2023

Revised: 23 December 2023

Accepted: 4 January 2024

Published: 8 January 2024



**Copyright:** © 2024 by the authors. Licensee MDPI, Basel, Switzerland. This article is an open access article distributed under the terms and conditions of the Creative Commons Attribution (CC BY) license (<https://creativecommons.org/licenses/by/4.0/>).

## 1. Introduction

The global market for electric vehicles and portable and wearable electronic devices is experiencing substantial growth, with an annual growth rate ranging from 10 to 25% [1]. The preferred energy storage devices for these applications are currently lithium-ion batteries [2]. This preference is attributed to their high energy and power density [2,3], lightweight nature [4], excellent cycle stability [5], and mature technology [6]. However, lithium-ion batteries come with drawbacks, including (i) a high cost due to limited natural resources [2] and relatively complex manufacturing [7], as well as (ii) safety concerns arising from the toxicity [8] and flammability of battery components and vent gas produced during thermal runaway [6,9]. Particularly for wearable or implantable devices, properties such as safety and biocompatibility are paramount for energy storage devices [10–13].

Several alternative batteries have been explored, involving monovalent metals like sodium [14–16] and potassium [17–19], as well as multivalent metals such as magnesium [20,21], calcium [22–24], zinc [7,25–27], and aluminum [28–31]. Aqueous zinc-ion batteries (ZIBs) are of particular interest due to their numerous advantages: (i) higher theoretical volumetric capacity of zinc metal (5854 mA h/cm<sup>3</sup>) compared to lithium metal

(2061 mA h/cm<sup>3</sup>) [32,33], (ii) higher energy density (1086 W h/kg) than lithium-ion batteries (about 300 W h/kg) [34], (iii) cost-effectiveness due to abundant zinc natural resources [25,35], (iv) efficient and scalable manufacturing facilitated by easy fabrication and absence of a glove box requirement, thanks to air-moisture-stable zinc electrodes [7,36], and (v) enhanced safety with non-toxic, biocompatible, non-flammable components using mildly acidic aqueous electrolytes, thanks to the low electrochemical redox potential of  $-0.763$  V versus the standard hydrogen electrode, which is compatible with aqueous electrolytes [7,25,27].

Despite their promising attributes, aqueous ZIBs face challenges, including (i) uneven zinc deposition causing dendrite formation and potential short-circuiting [37–40], (ii) cathode material dissolution and non-conductive byproduct formation shortening cycling life [41–43], (iii) water-induced side reactions leading to battery swelling [44], (iv) a narrow electrochemical stability window (about 1.23 V) increasing the risk of an oxygen evolution reaction [45], and (v) potential aqueous electrolyte leakage [46,47].

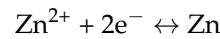
To address these challenges, replacing aqueous electrolytes with hydrogel polymer electrolytes for ZIBs has been proposed [47]. As far as the authors are aware of, hydrogel electrolytes were first introduced in ZIBs in 2017 with reported studies on a flexible rechargeable quasi-solid-state Zn-MnO<sub>2</sub> battery [48] and a smart flexible zinc battery [49]. Hydrogel electrolytes with reduced free water content and quasi-solid-state properties can suppress water splitting side reactions, zinc dendrite growth, electrode dissolution, and water leakage [50,51]. Moreover, hydrogel electrolytes enhance the stability of electrode–electrolyte interfaces through (i) the adhesion effect of hydrogel polar groups [50,52], (ii) close contact achievable with electrode active materials due to the mechanical elasticity of hydrogel electrolytes [53,54], and (iii) controlled Zn<sup>2+</sup> deposition through the interaction between Zn<sup>2+</sup> and hydrogel functional groups fixed in the hydrogel 3D network with evenly distributed ion transfer channels [55]. Hydrogels, with their hydrophilic polymer 3D network matrix, can hold aqueous electrolytes [56]. They can be tailored with different hydrophilic groups [57], 3D network structures [58], interesting porosity, and tunable mechanical strength and flexibility [59,60]. Hydrogel electrolytes can be derived from natural or synthetic materials [61,62], with most hydrogels exhibiting good biocompatibility and flexibility, making them suitable for contact with human skin, and implantable or digestible devices [63,64].

Despite successful applications, some aspects of hydrogel polymer electrolytes in ZIBs require further improvement for enhanced electrochemical performance. Notably, the discontinuous electrode–electrolyte interfacial contact in hydrogel ZIBs causes substantial interface impedance [65], resulting in higher activation energy for charge transfer and increased resistance for ion transport. This leads to non-uniform zinc ion diffusion and deposition during cycling. Moreover, hydrogel polymer electrolytes generally exhibit poor ionic conductivity in the range of  $10^{-5}$  to  $10^{-2}$  S cm<sup>-1</sup>, compared to about  $0.1$  S cm<sup>-1</sup> for aqueous electrolytes [66,67]. Lower ionic conductivity contributes to sluggish ion diffusion and mass transfer between electrodes during battery cycling, resulting in lower capacity and rate performance. Additionally, hydrogel polymer electrolytes have a relatively narrow electrochemical stability window [68] and are susceptible to aging effects [69]. Mechanical properties, such as structural strength, flexibility, and self-healing properties, are also critical for hydrogel polymer electrolytes [70,71].

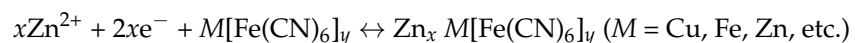
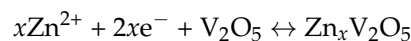
This review paper focuses on the advances over the past six years in the design and synthesis of hydrogel biopolymer electrolytes to improve the properties and performance of ZIBs, particularly through enhancing electrode–electrolyte interfaces. This paper provides an introduction to the energy storage mechanisms and the electrode–electrolyte interface in ZIBs, followed by sections on biopolymer hydrogel electrolytes and hybrid biopolymer–synthetic polymer hydrogel electrolytes, organized by biopolymer type. The final sections of the paper offer conclusions and future perspectives.

## 2. Energy Storage Mechanisms of Zinc-Ion Batteries

Aqueous ZIBs comprise the standard battery components, including a positive electrode, a negative electrode, an electrolyte, a separator, current collector(s), and a binder [72]. The binder facilitates the connection between the electrode and the current collector, whereas the separator acts as a physical barrier, ensuring the separation of electrodes and facilitating ion transport. The electrolyte's role is to enable ion transport between the positive and negative electrodes. Reversible zinc stripping and plating occur at the negative electrode during discharge and charge, respectively [73], and the charge storage mechanism at the Zn negative electrode can be expressed as follows:

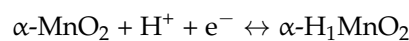


Various materials have been employed as positive electrodes in conjunction with hydrogel electrolytes, primarily including Mn-based oxides, V-based oxides, Prussian blue analogues (PBAs), carbon-based materials, and other active materials containing V or Zn. The storage mechanism at the positive electrode is debated, with several proposed mechanisms (Figure 1). The traditional mechanism involves  $\text{Zn}^{2+}$  insertion and extraction [74], reported for ZIBs with neutral electrolytes and various active materials, such as  $\text{MnO}_2$  polymorphs (both tunnel and layer structures),  $\text{V}_2\text{O}_5$ , vanadates, and PBAs [75–77]:



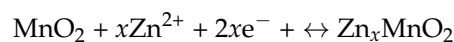
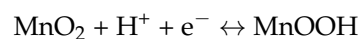
Zinc insertion can result in cathode crystal phase change and deliver high capacity for several  $\text{MnO}_2$  phases [78]. However, the diffusion kinetics are relatively slow due to the ionic size and strong electrostatic effect of  $\text{Zn}^{2+}$  ions, and Zn insertion can lead to rapid structural collapse of cathode materials [79].

The second mechanism involves proton insertion and extraction [80], where protons are inserted instead of  $\text{Zn}^{2+}$  ions in  $\text{MnO}_2$ :

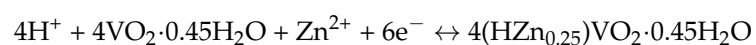


Proton insertion and extraction is energetically favored in Mn-based tunnel structures due to the small ionic radius and low electrostatic effects, facilitating fast diffusion and better stability [81]. However, extensive investigation is still required for proton insertion in different  $\text{MnO}_2$  polymorphs.

The third mechanism proposes dual-ion  $\text{Zn}^{2+}$  and  $\text{H}^{+}$  co-insertion, suggested for both tunnel- and layer-structured Mn-based cathodes in aqueous ZIBs [82]:



Studies indicated rapid proton insertion followed by slow zinc ion insertion, forming different Mn phases at varying voltages. Proton insertion generates a more alkaline solution and the formation of byproduct zinc hydroxide sulfate [83]. Similar sequential insertion mechanisms have been observed in vanadium dioxide cathodes [84] and vanadium hexacyanoferrate materials [85].



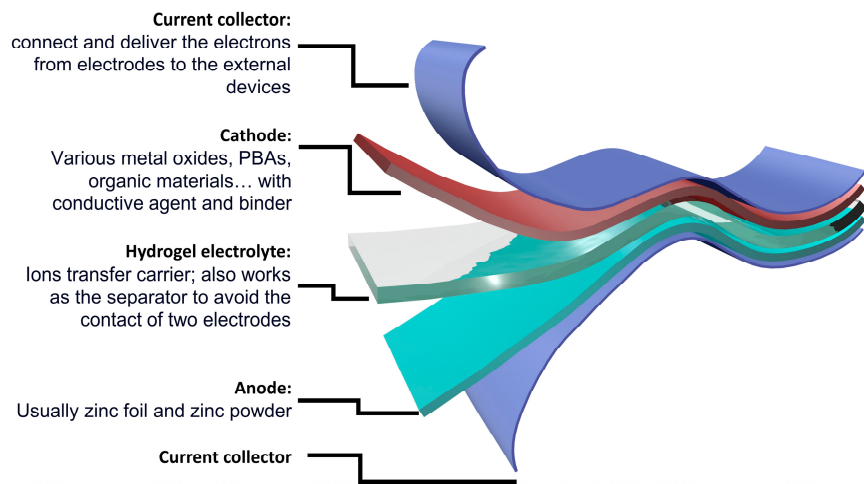
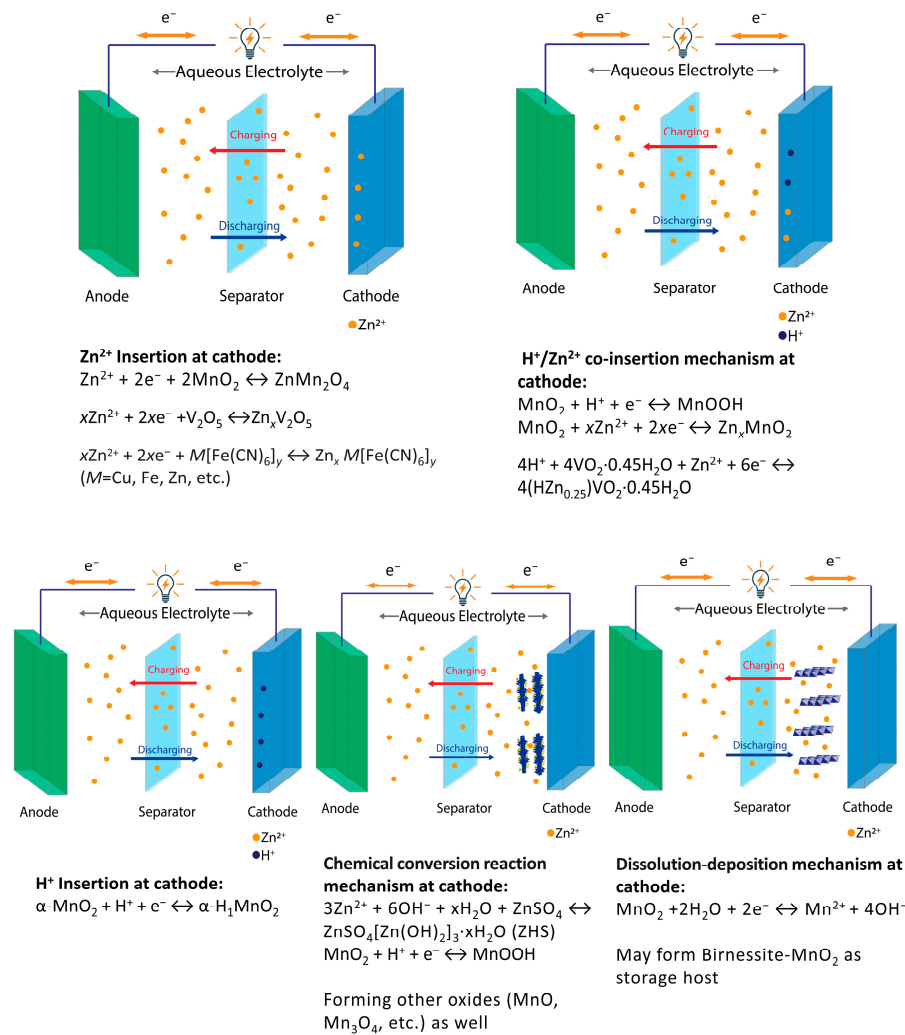
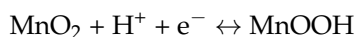


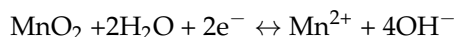
**Figure 1.** Top panel: Different storage mechanisms in common cathodes in ZIBs with hydrogel electrolytes. Bottom panel: Schematic diagram of a sandwich structure flexible ZIB and the functions of each component.

The fourth mechanism involves chemical conversion reactions, where  $\alpha\text{-}MnO_2$  reacts with protons to form MnOOH during discharging, and hydroxyl ions generate zinc hydroxide sulfate from the zinc sulfate electrolyte [86]. These reactions are reversed during charging, offering faster reaction kinetics compared to ion insertion mechanisms. However,

the chemical reactions vary among different electrolyte systems, and controlling reactions is essential to enhance cathode performance:



The fifth mechanism, dissolution–deposition, involves reversible dissolution and deposition of Mn-based cathode materials during the discharging and charging process, accompanied by the formation of byproducts [87]:



In summary, the mechanisms of ZIBs are intricate and contentious. Selecting appropriate active materials and further improving cathodes through the overall modification of the battery system may pave the way for enhanced electrochemical performance, especially in cells with hydrogel electrolytes.

### 3. Electrode–Electrolyte Interfaces in Zn-Ion Batteries

The performance and cycle life of rechargeable batteries are intricately tied to the electrode–electrolyte interfaces, encompassing both the cathode–electrolyte and anode–electrolyte interfaces. The voltage window of the battery is a critical determinant influenced by these interfaces, particularly noteworthy in batteries employing aqueous electrolytes, where the hydrogen evolution reaction can occur at the anode and the oxygen evolution reaction at the cathode [88]. These water-induced side reactions present significant challenges, as the hydrogen evolution reaction produces hydrogen gas, leading to electrolyte leakage and potentially battery failure. Furthermore, by depleting protons, this reaction can elevate pH levels at the interface, creating an alkaline environment conducive to the formation of  $\text{Zn}(\text{OH})_2$ . This, in turn, results in the deposition of insulating ZnO (via conversion) at the anode interface [89].

Hydrogel electrolytes exhibit dual functionality as both electrolytes and separators (Figure 1). Possessing properties that bridge the gap between liquids and solids, hydrogels offer excellent mechanical flexibility, strong adhesion, and reasonable ionic conductivity, and simultaneously reduce separator weight [90]. Consequently, the solid interface of hydrogel electrolytes acts as a physical barrier, effectively inhibiting cathode dissolution. At the anode side, hydrogel electrolytes play a crucial role in impeding dendrite formation. The hydrogel's design involves a trade-off, balancing a higher water content that enhances capacity with a lower water content that minimizes water decomposition and consequent ZnO formation at the anode, which would compromise the reversibility of Zn plating and stripping [91].

The stability of the interfaces in terms of their ability to withstand mechanical deformation is also important in batteries, since interfacial debonding results in capacity fade and higher impedance. Some insights on this matter can be derived from lithium-ion batteries. Simulations using the cohesive zone model showed that interfacial debonding between the active material particles and binder starts from the edge of the interface, propagating rapidly to the inner zone, and that it leads to a larger extent of the average state of charges in the particles because of the increased flux of ions through the new, debonded zones [92]. The state of charge and diffusion-induced stress evolution is significantly impacted by concentration-dependent local volume changes of the active material [93]. Moreover, this interfacial debonding is more probable in an electrode with a higher number of binder connections due to an increased amount of stress concentration locations [94]. Furthermore, previous research indicated that with growth of the solid electrolyte interface layer, tensile stress converts to compressive stress in the particles, resulting in a reduced probability of particle fracturing [95]. However, as the solid electrolyte interface starts fracturing, and

this fracturing is more pronounced on small particles than on large particles, then the probability of particle fracturing increases [95].

Notably, challenges at the electrode–electrolyte interface for hydrogel batteries center on the electrode–electrolyte contact and ion transport resistance. Various strategies have been proposed to address these challenges, including (i) modifying the cathode material to expand ion transport channels, (ii) tuning functional groups and side chains of hydrogel polymer electrolytes to induce uniform zinc deposition, and (iii) designing adhesive or self-sealable hydrogel polymer electrolytes to preserve the interface's integrity [51].

#### 4. Biopolymer Hydrogel Electrolytes for Zn-Ion Batteries

Numerous biobased materials have found application in the synthesis of hydrogel electrolytes for ZIBs, such as cellulose, carboxymethyl cellulose, alginate, chitosan, chitin, gelatin, guar gum, and xanthan gum. The primary aim of incorporating hydrogels in ZIBs is to mitigate zinc dendrite formation, suppress water-induced side reactions, expand the electrochemical stability window, enhance ionic conductivity, improve mechanical strength, widen operational conditions to subzero temperatures, extend service life, and enhance endurance under mechanical deformation. The use of biobased materials for these hydrogels is advantageous due to natural sourcing, cost-effectiveness, lightweight nature, and biodegradability. A summary of the investigated biopolymer hydrogel electrolytes for Zn-ion batteries with information on electrolyte type, mechanical strength, ionic conductivity and main advantages and disadvantages is presented in Table 1.

##### 4.1. Cellulose and Its Derivatives

Cellulose, the most abundant natural polymer, is a linear polysaccharide constituting the main component of plant skeletal structures [96]. It consists of a repetition of D-glucose building blocks that are connected via  $\beta$ -1,4-glycosidic bonds [61]. Characterized by its hydrophilic, non-toxic, and biodegradable nature [96], cellulose serves as an ideal candidate for hydrogel electrolytes in ZIBs.

##### 4.1.1. Enhanced Mechanical and Electrochemical Properties

To capitalize on the mechanical strength of cellulose, hydrogel electrolytes have been developed to enhance both mechanical and electrochemical properties for ZIBs. A common synthesis procedure involves preparing a cellulose hydrogel followed by immersion in a zinc sulfate solution to form the hydrogel electrolyte. For instance, ultrathin (about 10  $\mu\text{m}$ ) cellulose hydrogel electrolyte membranes were fabricated for ZIBs with the  $\text{V}_2\text{O}_5$  cathode, exhibiting impressive tensile strength (39.5 MPa), reasonable ionic conductivity ( $0.643 \text{ mS cm}^{-1}$ ), and a wide electrochemical window (1.6 V) [97]. The cellulose gel membranes were created by dissolving paper scraps in a lithium chloride and *N,N*-dimethylacetamide solution through stirring at 100 °C. Subsequent steps involved drying on a hot plate at 60 °C, rinsing, and vacuum oven drying at 60 °C [97]. The resulting cellulose gel membranes were cut and immersed in a 3 M  $\text{ZnSO}_4 \cdot \text{H}_2\text{O}$  solution to achieve the hydrogel electrolyte [97]. This procedure generated a hydrogel electrolyte with a dense structure and low thickness, effectively reducing the ion transfer distance. Moreover, the hydrogels exhibited superior dendrite inhibition compared to traditional separators due to the enhanced compatibility with the zinc anode and the non-porous structure. The resulting ZIBs delivered a maximum capacity of about 400 mAh  $\text{g}^{-1}$  after 10 cycles at a current density of 0.1 A  $\text{g}^{-1}$ , and a capacity retention rate of 62.5% after 200 cycles [97]. The ZIBs demonstrated excellent electrochemical stability over 2000 cycles with nearly 100% Coulombic efficiency [97].

Bacterial cellulose, with its interconnected network structure [98], was employed as a hydrogel electrolyte for ZIBs with a cathode made of carbon nanofibers on  $\text{Mn}_3\text{O}_4$ , achieved through the carbonization of bacterial cellulose pre-absorbed with Mn salt [98]. The resulting carbonized porous bacterial cellulose, forming a 3D network structure, provided numerous ion pathways. The hydrogel, derived from bacterial cellulose from *Nata-de-coco*

via freeze drying, alkali treatment, and immersion in an aqueous solution of 2.0 M ZnSO<sub>4</sub> and 0.2 M MnSO<sub>4</sub>, exhibited high ionic conductivity (27.8 mS cm<sup>-1</sup>) [98]. ZIBs with this hydrogel electrolyte achieved a specific capacity of 415.2 mAh g<sup>-1</sup> at 0.1 A g<sup>-1</sup>, excellent Coulombic efficiency of more than 99%, and a capacity retention of 88.2% after 1000 cycles at a current density of 2 A g<sup>-1</sup> [98].

Incorporating the principles of the Hofmeister effect (Figure 2), high-concentration kosmotropic ions were introduced into a cellulose hydrogel, exploiting the salting-out effect [53]. Carboxymethyl cellulose (CMC) was selected for its negatively charged framework, good solubility in water, and abundant oxygen-containing functional groups [53]. The hydrogel was produced by adding acetic acid to the CMC solution to facilitate gelation, followed by four freeze–thaw cycles, and drying at room temperature [53]. Subsequently, the hydrogel film was immersed in an aqueous solution of 7 M KAc and 1 M ZnAc<sub>2</sub> [53]. The generated hydrogel electrolyte displayed a wide electrochemical window (up to 2.3 V), facilitated by the high concentration of acetates that modified the solvation shell of the electrolyte solvent and reduced the active water molecules. Furthermore, the hydrogel exhibited a tensile strength of 1.33 MPa, fracture elongation of 185%, and ionic conductivity of 34.5 mS cm<sup>-1</sup> [53]. This hydrogel demonstrated not only targeted improvements but also good adhesion, water retention, dendrite suppression, and resistance to water-induced side reactions [53]. Pouch cell Zn/polyaniline batteries with this CMC hydrogel electrolyte showed a capacity of 145.7 mAh g<sup>-1</sup> at 0.2 A g<sup>-1</sup> after 10 cycles, retaining 79.5% capacity after 2000 cycles at 1 A g<sup>-1</sup> [53].

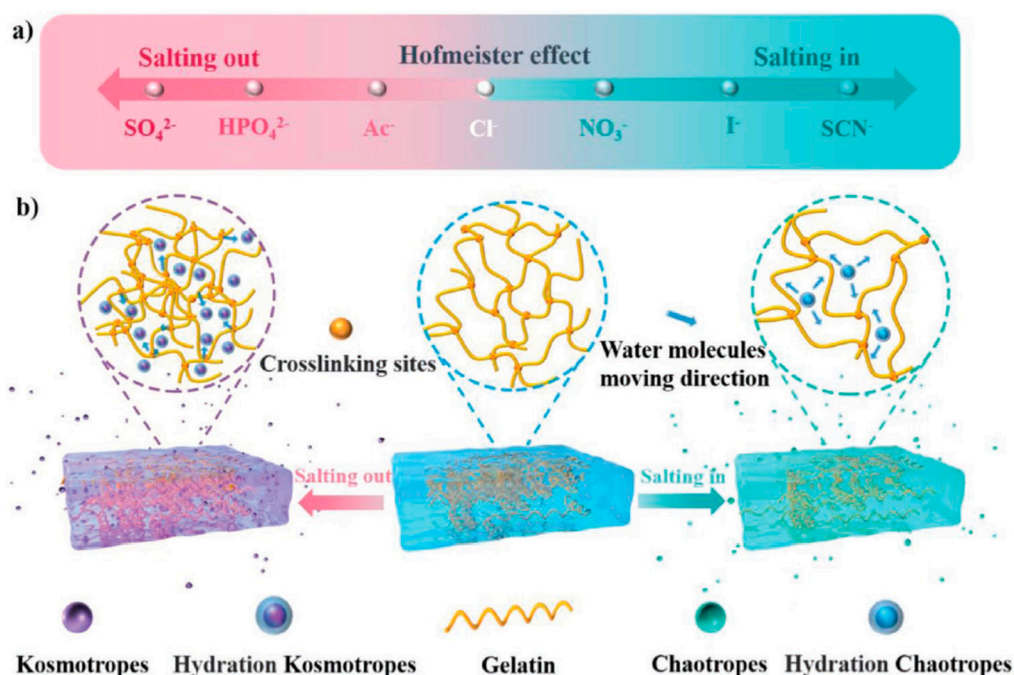


**Figure 2.** Hofmeister effect with Hofmeister series for anions (a) and salting-out and salting-in effects illustrated for hydrogel with kosmotropic ions and with chaotropic ions, respectively (b). Figure from [99] reprinted with permission.

#### 4.1.2. Improved Cycling Stability

In pursuit of enhanced cycling stability, a nanocellulose–carboxymethyl cellulose hydrogel electrolyte was developed (Figure 3) [100]. This involved dispersing 0.1 wt% commercial cellulose nanofiber gel in deionized water, adding a 5 wt% CMC solution, and subjecting the dispersion to vacuum filtration [100]. The produced membranes were immersed in a 20 wt% NaOH aqueous solution and later in an aqueous solution of 2 M ZnSO<sub>4</sub> [100]. The resulting hydrogel electrolyte exhibited a high tensile strength of 70 MPa, ionic conductivity of 26 mS cm<sup>-1</sup>, and excellent dendrite suppression due to controlled Zn<sup>2+</sup>

movement facilitated by the affinity of water with the CMC main chain [100]. ZIBs with this hydrogel electrolyte and a  $\text{MnO}_2$  cathode delivered a specific capacity of about  $200 \text{ mAh g}^{-1}$  at a current density of  $2 \text{ A g}^{-1}$ , with a capacity retention of 95% after 500 cycles [100].

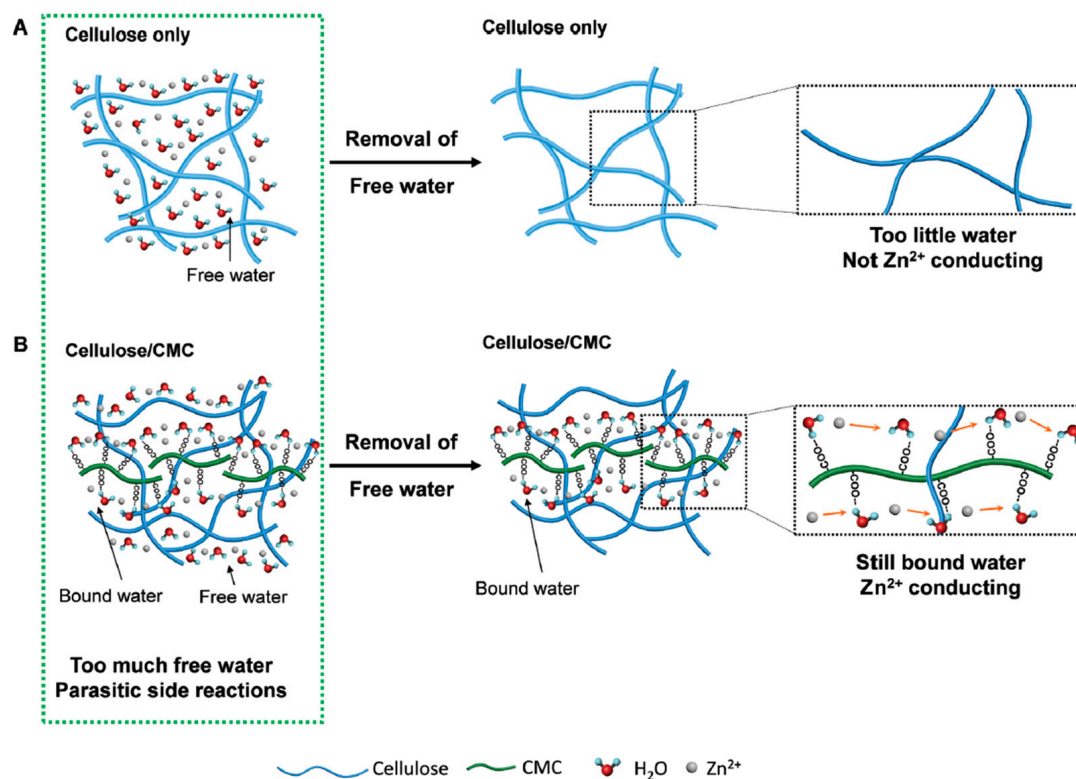


**Figure 3.** Schematic diagram illustrating the difference between cellulose-only hydrogel (A) and cellulose-CMC hydrogel (B). For both hydrogels, parasitic side reactions are induced in the case of too much free water. However, with the removal of free water, the ionic conductivity becomes too low for cellulose-only hydrogel in contrast to cellulose-CMC hydrogel. Figure from [100] reprinted with permission.

Another study aimed to enhance the lifespan of ZIBs by employing CMC in a hydrogel electrolyte, mixed with agarose and 4 wt% glutaraldehyde for cross-linking [101]. The resulting hydrogel electrolyte, immersed in an aqueous 2 M  $\text{ZnSO}_4$  solution, demonstrated stable electrode–electrolyte interface properties due to even zinc ion diffusion facilitated by the abundant polar groups in the hydrogel. ZIBs with this hydrogel electrolyte and a polydopamine-based cathode exhibited a capacity of  $196 \text{ mAh g}^{-1}$  after 1000 cycles at a current density of  $0.5 \text{ A g}^{-1}$ , and a capacity of  $110 \text{ mAh g}^{-1}$  after 10,000 cycles at a current density of  $1 \text{ A g}^{-1}$  (Figure 4) [101].

In a coaxial-fiber design for flexible, high-voltage rechargeable ZIBs, CMC was utilized in a hydrogel electrolyte [102]. The hydrogel electrolyte, formed by dissolving CMC and  $\text{ZnSO}_4 \cdot 7\text{H}_2\text{O}$  in distilled water under stirring at  $85^\circ\text{C}$ , contributed to the assembly of fiber ZIBs with a zinc hexacyanoferrate cathode [102]. The resulting fiber ZIBs achieved a capacity of  $100.2 \text{ mAh cm}^{-3}$  at a current density of  $0.1 \text{ A cm}^{-3}$ , an energy density of  $195.4 \text{ mWh cm}^{-3}$  at a power density of  $0.2 \text{ A cm}^{-3}$ , and a capacity retention of 93.2% after 3000 bending cycles [102].

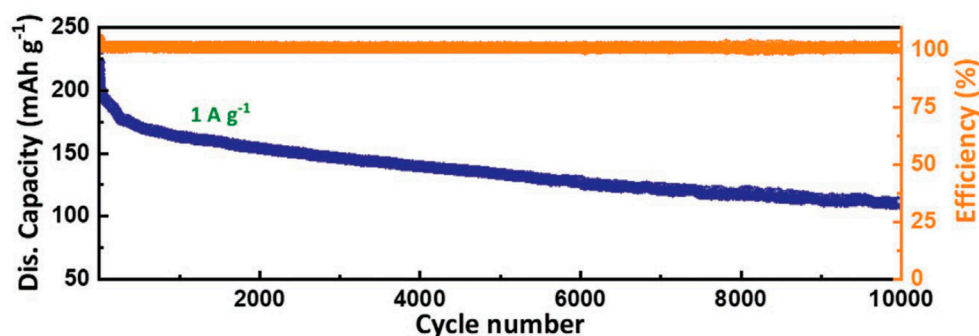


**Figure 4.** Long-term cycling performance, with discharging capacity on the left axis and Coulombic efficiency on the right axis, for ZIB with CMC-based hydrogel electrolyte at  $1 \text{ A g}^{-1}$  over 10,000 cycles. Figure slightly modified from [101] reprinted with permission.

#### 4.1.3. Anti-Freezing Properties

Hydrogel electrolytes with anti-freezing properties were developed for ZIBs using cotton as a raw material. This cost-effective approach involved adding tetraethyl orthosilicate as a cross-linker and glycerol as an anti-freezing agent (Figure 5) [103]. Cotton was treated with an alkali solution, ground, and dissolved in an aqueous  $\text{ZnCl}_2$  solution [103]. Glycerol was then added, followed by the cross-linker, to form a 3D porous network via covalent siloxane bonds [103]. The hydroxyl groups in the CMC skeleton inhibited the crystallization of water molecules and promoted the distribution of glycerol through the cross-link of siloxane bonds, contributing a stable ion transfer pathway. The resulting hydrogel electrolyte exhibited an ionic conductivity of  $19.4 \text{ mS cm}^{-1}$  at  $-40 \text{ }^\circ\text{C}$ , and effectively suppressed zinc dendrite formation and water-induced side reactions over a temperature range of  $-40$  to  $60 \text{ }^\circ\text{C}$  [103]. ZIBs with this hydrogel electrolyte and a  $\text{MnO}_2$  cathode demonstrated a specific capacity of  $277.3 \text{ mAh g}^{-1}$  at a current density of  $0.2 \text{ A g}^{-1}$ , a capacity retention of 99.2% after 2000 cycles at  $20 \text{ }^\circ\text{C}$ , a Coulombic efficiency of 99.9%, and excellent performance under harsh conditions, including bending, water immersion, and low temperature [103].

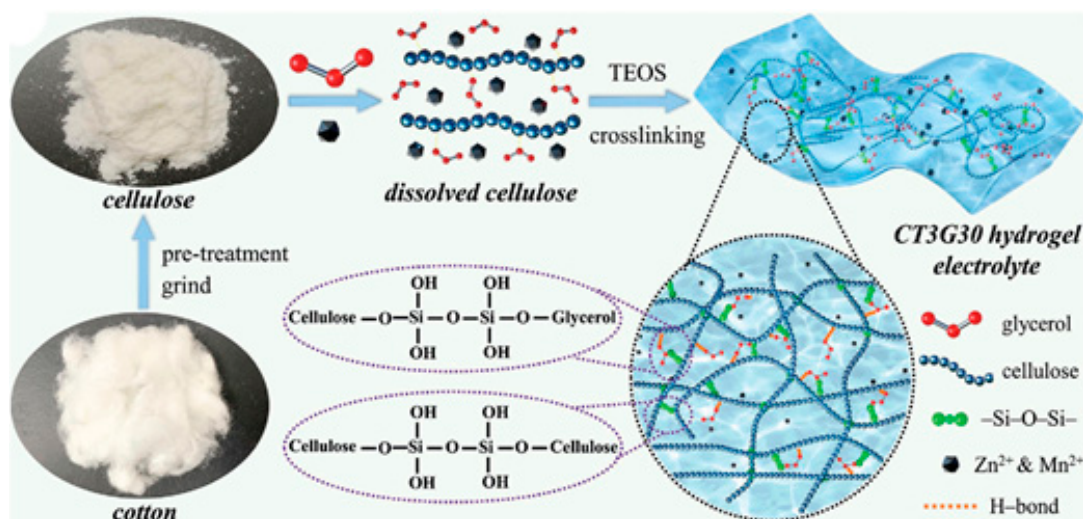


**Figure 5.** Schematic diagram displaying the synthesis procedure to fabricate the cotton-derived hydrogel with anti-freezing properties, involving pre-treatment, dissolution, and cross-linking steps. Figure slightly modified from [103] reprinted with permission.

In another study, a sorbitol-modified cellulose hydrogel electrolyte was developed for a flexible Zn-polyaniline ZIB [52]. Cellulose was extracted from ground and ball-milled wheat straw treated with a  $\text{NaOH}$  and  $\text{H}_2\text{O}_2$  solution, UV radiation, and freeze drying. The extracted cellulose was dissolved in an aqueous solution of  $16 \text{ M ZnCl}_2$  (to achieve

water-in-salt effect) and 0.6 M  $\text{CaCl}_2$  (which can act as a gelling agent) under stirring at  $65^\circ\text{C}$ , and sorbitol was added as a cryoprotectant [52]. The resulting hydrogel electrolyte exhibited a tensile strength of 0.62 MPa, a fracture elongation of 303%, strong adhesion, an ionic conductivity of  $35.4\text{ mS cm}^{-1}$  at  $20^\circ\text{C}$ , and a very low freezing point of  $-101.5^\circ\text{C}$  [52]. Sorbitol facilitated desolvation of hydrated zinc ions, suppressing water-induced side reactions and enhancing zinc deposition kinetics. Moreover, sorbitol formed hydrogen bonds with the cellulose polymer, promoting gelation. ZIBs in this study delivered a capacity of  $114.4\text{ mAh g}^{-1}$  at a current density of  $0.2\text{ A g}^{-1}$ , and the capacity retention was 74.9% for 1000 cycles at a current density of  $1\text{ A g}^{-1}$  and a temperature of  $20^\circ\text{C}$  [52].

#### 4.2. Chitin and Chitosan

Chitin, the second most abundant natural polymer, is a polysaccharide found in the exoskeleton of arthropods or the cell walls of fungi and yeast [104]. It consists of polymer chains with repetitive units of *N*-acetyl-D-glucosamine connected via  $\beta$ -(1→4) linkages [104]. Chitosan, a deacetylated form of chitin with approximately 50% deacetylation, is a random copolymer comprising *N*-acetyl-D-glucosamine and D-glucosamine, and is water-soluble [104].

The development of hydrogel electrolytes based on chitin or chitosan aims to enhance the safety, sustainability, and biodegradability of ZIBs, while also suppressing zinc dendrite formation for improved electrochemical performance and cycling life. For instance, a chitosan-Zn membrane electrolyte was prepared by dissolving 0.5 wt% chitosan powder in a 4 wt% acetic acid aqueous solution under stirring at room temperature. Subsequently, filtration and evaporation were employed to achieve a 4 wt% chitosan solution [105]. The resulting porous chitosan-Zn membrane, obtained by immersing the chitosan wet film in an aqueous 20 wt% NaOH solution with 0.6 wt% Zn ions for four days, was washed, and the electrolyte was prepared by immersing the membrane in a 2 M  $\text{ZnSO}_4$  aqueous solution [105]. A pressure of about 5 MPa was applied to densify the membrane, resulting in smaller surface area and lower free water content due to the hydrogen bonding between hydrophilic groups in chitin and water [105]. Those electrolytes showed an ionic conductivity of  $71.8\text{ mS cm}^{-1}$  at a water content of 57% [105]. ZIBs employing this electrolyte and a polybenzoquinonyl sulfide (PBQS) organic cathode delivered a capacity of  $190\text{ mAh g}^{-1}$  at a current density of  $1\text{ A g}^{-1}$  and exhibited a capacity retention of 71% after 400 cycles (Figure 6) [105].

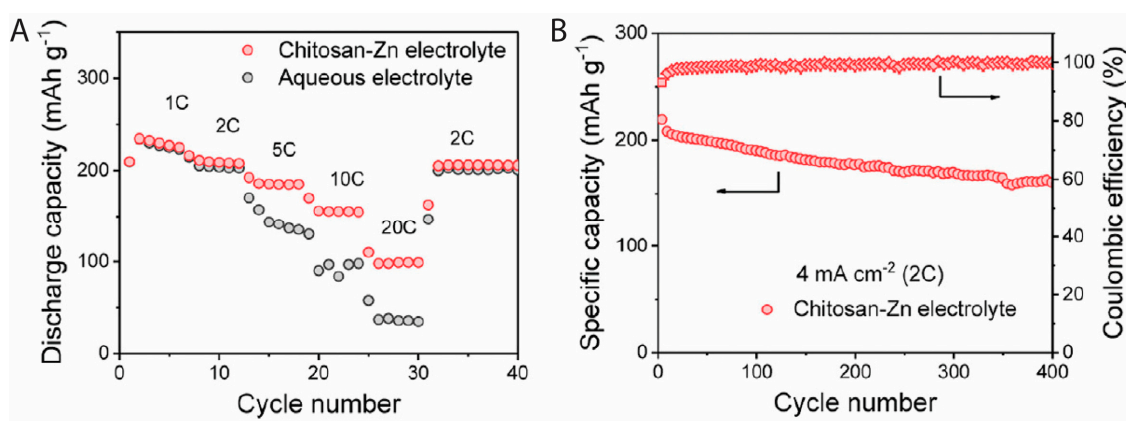


**Figure 6.** (A) Rate performance for the ZIB with PQBS cathode at rates ranging from 1 to 20C, comparing the ZIB with aqueous electrolyte and that with the chitosan-based hydrogel electrolyte. (B) Cycling performance, with specific capacity on the left axis and Coulombic efficiency on the right axis, of the ZIB with the chitosan-based hydrogel electrolyte at 2C with a PBQS loading of  $10\text{ mg cm}^{-2}$ . Figure slightly modified from [105] reprinted with permission.

In another study, a chitosan-based hydrogel electrolyte was developed to regulate zinc deposition and suppress dendrite formation in rechargeable ZIBs [106]. The hydrogel was

prepared by purifying and dissolving chitosan in acetic acid, pouring it onto a glass fiber separator, and neutralizing it through immersion in a NaOH solution of pH 10 [106]. The chitosan glass fiber membrane was then immersed in a 2 M ZnSO<sub>4</sub> aqueous solution to enable cross-linking and hydrogel electrolyte formation [106]. With a mechanical strength of 2.4 MPa, the hydrogel membrane inhibited zinc dendrite penetration [106]. ZIBs using this electrolyte and a NaV<sub>3</sub>O<sub>8</sub> cathode delivered a capacity of 275.8 mAh g<sup>-1</sup> at a current density of 0.5 A g<sup>-1</sup>, indicating fast ion transport in the hydrogel. The ZIBs exhibited a capacity retention of 31% after 500 cycles at a current density of 2 A g<sup>-1</sup> [106].

An additional approach to developing dendrite-free ZIBs utilizing chitosan-based hydrogel involved modifying cotton pad separators [107]. Following a similar procedure to the previous study, the glass fiber membrane was replaced with a cotton pad separator [107]. In Zn symmetric cells with the chitosan hydrogel cotton pad separator, a cycling longevity of 1500 h was achieved at a current density of 1 mA cm<sup>-2</sup>, and 600 h at a current density of 4 mA cm<sup>-2</sup> [107]. The high mechanical strength of chitosan-based hydrogel prevented puncturing by zinc dendrites. Moreover, water-induced side reactions and zinc deposition were controlled through favorable adsorption of free water and zinc ions on the functional groups in chitosan. ZIBs with this hydrogel electrolyte separator and a NaV<sub>3</sub>O<sub>8</sub> cathode delivered a specific capacity of 102.0 mAh g<sup>-1</sup> after 700 cycles at a current density of 1 A g<sup>-1</sup> [107].

In a study on the development of green ZIBs, polyaspartic acid was used instead of acetic acid in the chitosan-based hydrogel preparation procedure (Figure 7) [108]. The hydrogel, prepared by dissolving 6 wt% chitosan and 1 wt% polyaspartic acid (PASP) (both sourced from snail shells) in an aqueous solution of 9 wt% NaOH and 18 wt% urea, exhibited increased porous structures [108]. Moreover, the carboxyl groups in PASP acted as additional hopping sites promoting mass transfer. ZIBs using this electrolyte and a MnO<sub>2</sub> cathode showed a capacity of 523.6 mAh g<sup>-1</sup> at a current density of 0.1 A g<sup>-1</sup>, a capacity retention of 92.5% over 5000 cycles, and an energy density of 452.2 Wh kg<sup>-1</sup> even at a high power density of 753.6 W kg<sup>-1</sup> [108].

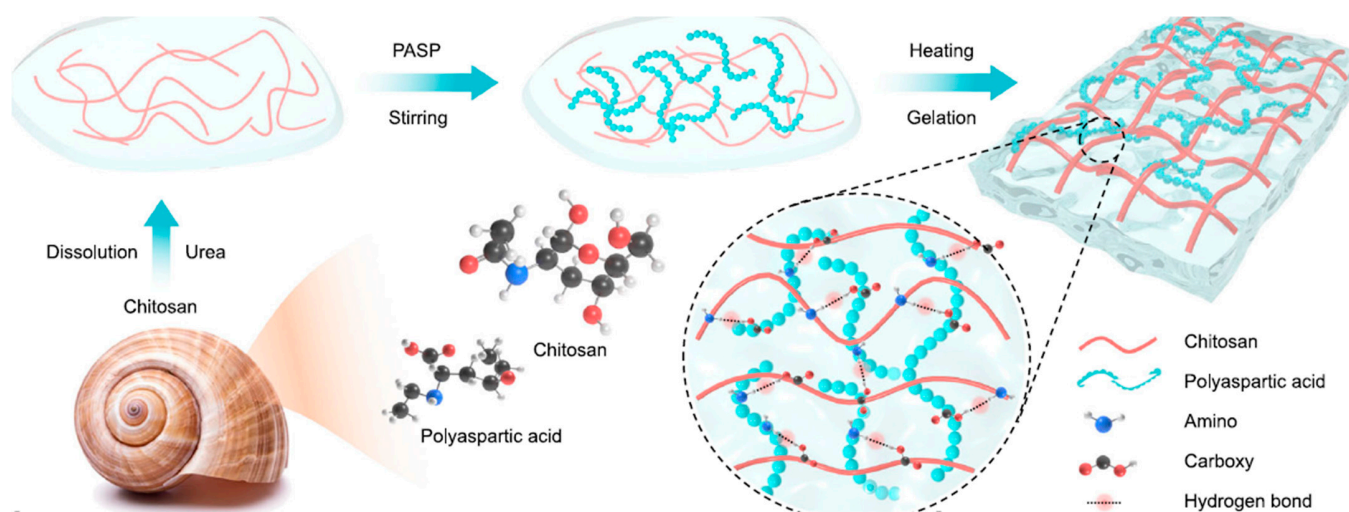


**Figure 7.** Schematic diagram illustrating the synthesis process to create the chitosan-based hydrogel electrolyte with polyaspartic acid, involving dissolution, mixing, and gelation steps. Figure slightly modified from [108] reprinted with permission.

Chitosan and carrageenan were synergistically combined to create a hydrogel electrolyte designed for “open” pouch cells targeting large-scale-capacity ZIBs [109]. The hydrogel electrolyte, made by dissolving 0.1 wt% chitosan in deionized water and dispersing 1 wt% k-carrageenan in the saturated chitosan solution, followed by casting and subsequent immersion in a 2 M ZnSO<sub>4</sub> aqueous solution, exhibited ionic conductivity of 5.3 mS cm<sup>-1</sup> at room temperature [109]. The polar functional groups in this hybrid elec-

trolyte suppressed the free water and water-related side reactions. The open cell structure enabled water refilling, and the pouch symmetric cells achieved a lifetime of about 4000 h and a capacity of 35 mAh cm<sup>-2</sup> at 10 mA cm<sup>-2</sup> [109]. Coin cell ZIBs with this hydrogel electrolyte and a Zn<sub>x</sub>V<sub>2</sub>O<sub>5</sub>·*n*H<sub>2</sub>O cathode delivered a specific capacity of 349.6 mAh g<sup>-1</sup> at a current density of 0.2 A g<sup>-1</sup>, with a capacity retention of 88.2% after 100 cycles [109].

A thermosensitive reversible electrolyte was prepared using modified chitin for the development of aqueous ZIBs, preventing thermal runaway by changing to a gel state at higher temperatures, inhibiting zinc ion migration [110]. The electrolyte was prepared by dissolving chitin in an aqueous solution of 11 wt% NaOH and 4 wt% urea, followed by the addition of iodomethane [110]. Subsequently, the methylated chitin was dissolved in a 20 wt% NaOH aqueous solution, then iodomethane was added at 20 °C, followed by neutralization, dialysis, and freeze drying [110]. The electrolyte, produced by dissolving the prepared methylated chitin in distilled water and mixing it with 2 M ZnSO<sub>4</sub> and 0.1 M MnSO<sub>4</sub>, exhibited reversible temperature responsiveness, attributed to the hydrogen bonding and interaction of functional groups [110]. The gelation process inhibited ion transfer and controlled reaction speed. ZIBs with this electrolyte and α-MnO<sub>2</sub> cathode demonstrated decreased capacity from 143.9 mAh g<sup>-1</sup> at 35 °C to 2.4 mAh g<sup>-1</sup> at 75 °C, with an energy density decrease from 199.7 Wh kg<sup>-1</sup> to 2.4 Wh g<sup>-1</sup> for the same temperature change [110].

#### 4.3. Alginate

Alginate, a polysaccharide biomaterial, is naturally found in the outer cell walls of brown algae [111]. Comprising linear copolymers, alginate consists of blocks of (1,4)-linked β-D-mannuronate and α-L-guluronate residues, and is renowned for its biocompatibility and gelation properties [111].

In the pursuit of highly reversible ZIBs with dendrite-free zinc anodes, a hierarchically three-dimensional gel electrolyte was developed from alginate by cross-linking zinc ions with alginate carboxylate groups [112]. The hydrogel electrolyte synthesis involved dissolving sodium alginate in deionized water, followed by stirring under a vacuum and immersion in an aqueous solution of 2 M ZnSO<sub>4</sub> and 0.2 M MnSO<sub>4</sub> to facilitate the cross-linking reaction [112]. The alginate hydrogel exhibited a restriction of zinc ion migration due to the carboxylate groups, leading to an ionic conductivity of 18.3 mS cm<sup>-1</sup> at room temperature [112]. ZIBs utilizing this hydrogel electrolyte and an α-MnO<sub>2</sub> cathode achieved a capacity of 300 mAh g<sup>-1</sup> at a current density of 0.2 A g<sup>-1</sup>, maintaining nearly 100% Coulombic efficiency over 100 cycles, along with acceptable cycling stability and rate capability [112].

A recent study reported the synthesis of a zinc alginate hydrogel electrolyte to develop dendrite-free ZIBs with reduced interfacial resistance [113]. The zinc alginate hydrogel was prepared via solution casting, involving the dissolution of sodium alginate in ultrapure water under stirring, followed by drying on a hot plate at 50 °C, and immersion of the alginate membrane in a 3 M ZnSO<sub>4</sub> aqueous solution [113]. The resulting zinc alginate hydrogel electrolyte exhibited excellent mechanical properties, a dense structure for even ionic distribution, and reduced side reactions and dendrite growth. With an ionic conductivity of 1.24 mS cm<sup>-1</sup> at room temperature, ZIBs employing this electrolyte and a Ca<sub>0.24</sub>V<sub>2</sub>O<sub>5</sub> cathode demonstrated stable cyclability for 600 cycles at a current density of 1.2 A g<sup>-1</sup>, with a capacity retention of 88.7% [113].

Additionally, alginate was employed to create a self-healing and self-adapting hydrogel interface with a zinc anode, promoting fast ion transport in ZIBs [114]. The hydrogel electrolyte was produced by coating the zinc anode with sodium alginate, which was then converted in situ to zinc alginate hydrogel through immersion in an aqueous ZnSO<sub>4</sub> solution. This process, involving the replacement of sodium ions with zinc ions, enabled linking with carboxyl groups and cross-linking, resulting in gelation [114]. The carboxyl groups, with a negative charge, facilitated desolvation through an affinity to zinc cations and repulsion of SO<sub>4</sub><sup>-</sup> anions. The hydrogel electrolyte demonstrated an ionic conductivity

of  $0.54 \text{ mS cm}^{-1}$  [114]. ZIBs using this electrolyte and a  $\text{MnO}_2$  cathode delivered a capacity of  $214 \text{ mAh g}^{-1}$  at 2C after 500 cycles [114].

In certain studies, sodium alginate was reacted with other chemicals in addition to zinc sulfate. For instance, a cross-linked composite hydrogel of sodium alginate with tannic acid was developed and used in ZIBs with a  $\text{NH}_4\text{V}_4\text{O}_{10}$  cathode [115]. The hydrogel electrolyte was prepared by mixing sodium alginate and tannic acid in deionized water, followed by immersion in 2 M  $\text{ZnSO}_4$  to achieve cross-linking between  $\text{Zn}^{2+}$  and  $-\text{COO}^-$  groups from sodium alginate and chelation with  $-\text{OH}$  groups from tannic acid [115]. The full cell delivered a capacity of  $238.6 \text{ mAh g}^{-1}$  and a capacity retention of 94.5% after 900 cycles at  $2 \text{ A g}^{-1}$  (Figure 8) [115].

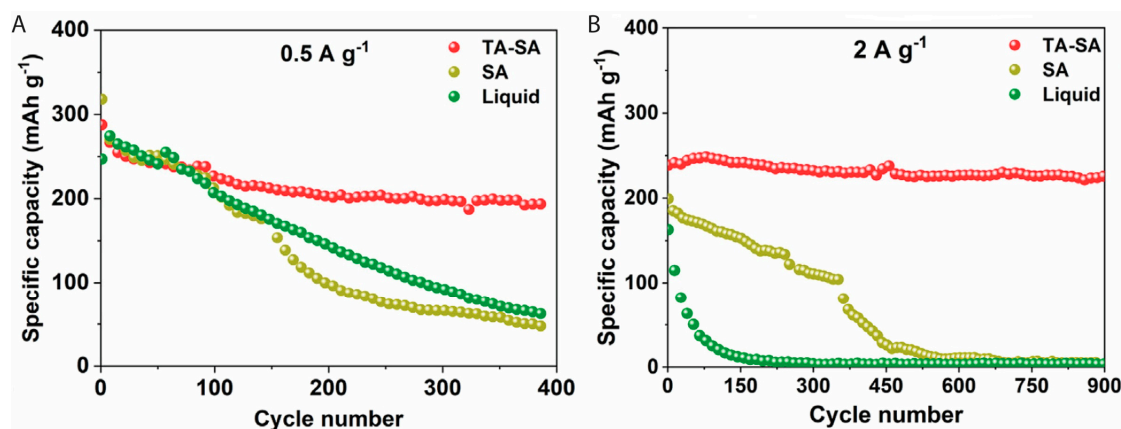


**Figure 8.** Comparison between the cycling performance of ZIBs with aqueous electrolyte, sodium-alginate-based hydrogel electrolyte, and tannic acid–sodium alginate hydrogel electrolyte. (A) Cycling performance at  $0.5 \text{ A g}^{-1}$ . (B) Long-term cycling performance at  $2 \text{ A g}^{-1}$ . The tannic acid–sodium alginate hydrogel electrolyte maintains excellent performance over 900 cycles. Figure slightly modified from [115] reprinted with permission.

In another study, a hydrogel was prepared with sodium alginate, guar gum, and ethylene glycol to create flexible and anti-freezing ZIBs [116]. A mixture of 4 wt% sodium alginate and 2 wt% guar gum was created in an aqueous solution of 2 M  $\text{ZnSO}_4$  and 0.1 M  $\text{MnSO}_4$  under stirring at room temperature [116]. After casting and air-drying, the hydrogel electrolyte was immersed in a 30 vol% ethylene glycol (EG) solution with 2 M  $\text{ZnSO}_4$  and 0.1 M  $\text{MnSO}_4$  [116]. The hydrogel exhibited an ionic conductivity of  $16.81 \text{ mS cm}^{-1}$  at  $25 \text{ }^\circ\text{C}$ , and  $6.19 \text{ mS cm}^{-1}$  at  $-20 \text{ }^\circ\text{C}$  [116]. This result indicates that the introduction of EG significantly decreases the freezing points of hydrogels through abundant intermolecular hydrogen bonding between EG and water. ZIBs with this hydrogel delivered a capacity of  $135 \text{ mAh g}^{-1}$  at a current density of  $3 \text{ A g}^{-1}$ , with a capacity retention of 78.3% over 1000 cycles at  $6 \text{ A g}^{-1}$  at room temperature [116]. The ZIBs operated at  $-20 \text{ }^\circ\text{C}$  with a capacity of  $181.5 \text{ mAh g}^{-1}$  at a current density of  $0.1 \text{ A g}^{-1}$  [116].

Alginate was also combined with chitosan in research on the development of green and scalable hydrogel electrolytes for ZIBs (Figure 9) [117]. The hydrogel solutions were created through microfluidic mixing of aqueous solutions of sodium alginate and chitosan with  $\text{ZnCl}_2$  salt, followed by centrifugation to concentrate and separate the hydrogel electrolyte [117]. The produced hydrogel electrolyte had an ionic conductivity of about  $10 \text{ mS cm}^{-1}$  and demonstrated a stable interface with Zn electrodes in a symmetric cell, operating for more than 7000 galvanostatic cycles [117].

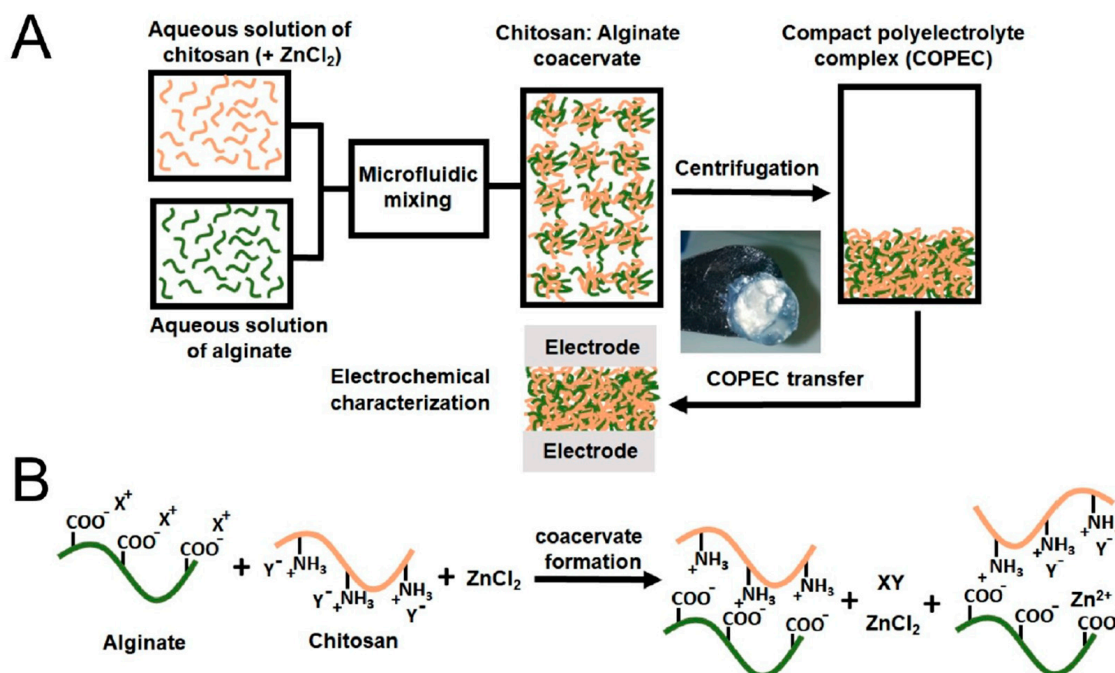


**Figure 9.** Alginate–chitosan hydrogel electrolyte. (A) Preparation method illustrating microfluidic mixing, centrifugation, and transfer steps, followed by electrochemical characterization. (B) Targeted ionic interactions between alginate and chitosan in the hydrogel electrolyte. Figure from [117] reprinted with permission.

#### 4.4. Gelatin

Gelatin, a widely used biopolymer, finds applications in diverse fields such as biomedical, pharmaceutical, food, and cosmetics [118]. Derived from the partial hydrolysis of collagen, a fibrous protein constituting a major component of connective tissues, skin, and bone, gelatin is not naturally occurring [119].

In the pursuit of enhanced safety and stability, flexible ZIBs have been developed with gelatin-based hydrogel electrolytes [60]. The hydrogel electrolyte was prepared by dissolving 10 wt% gelatin in an aqueous solution with 0.5 M Li<sub>2</sub>SO<sub>4</sub> and 0.5 M ZnSO<sub>4</sub> under stirring at 60 °C, followed by casting and cooling in a cryogenic box [60]. Exhibiting an ionic conductivity of 37.2 mS cm<sup>-1</sup> and a mechanical strength of approximately 50 kPa with a corresponding strain of 50% at a temperature of 25 °C, the hydrogel facilitated ZIBs with a LiMn<sub>2</sub>O<sub>4</sub> cathode to achieve a capacity of 110 mAh g<sup>-1</sup> and a capacity retention of 89% after 200 cycles at a current density of 0.1 A g<sup>-1</sup> [60]. The hydrogel's protective role against water corrosion and side reactions contributed to the high stability of the cell, even when subjected to bending, twisting, or immersion in water [60]. Nevertheless, the relatively low mechanical strength may hinder its further application as an electrolyte in ZIBs.

In another study, a gelatin-based electrolyte was employed to produce ultra-stable ZIBs with a MnO<sub>2</sub> cathode [120]. Gelatin powder, dissolved at 10 wt% in an aqueous solution under stirring at 60 °C, was poured into a mold and rapidly cooled to 1 °C, followed by immersion in a ZnSO<sub>4</sub>/MnSO<sub>4</sub> mixed aqueous solution [120]. The high concentration of inorganic salt induced a salt-reinforced effect, resulting in strong hydrophobic interactions and enhanced main chain strength in the hydrogel. Consequently, the hydrogel exhibited a mechanical tensile strength of 2.78 MPa [120]. ZIBs utilizing this hydrogel electrolyte and an α-MnO<sub>2</sub> cathode demonstrated a specific capacity of 285 mAh g<sup>-1</sup> at 0.1C, with a capacity retention of 90% after 500 cycles at 5C [120]. The study reported no capacity loss after bending 200 times, and immersion in water had no adverse effects on the battery's performance [120].

Similarly, flexible ZIBs were developed with gelatin-based electrolytes to achieve superior mechanical and electrochemical performance [99]. In this case, the electrolyte was prepared by dissolving 10 wt% gelatin in water at 70 °C, followed by cooling in a refrigerator to obtain a pre-frozen gelatin hydrogel, which was subsequently immersed in an aqueous solution of 2 M ZnSO<sub>4</sub> [99]. Various zinc salts were tested for synthesizing hydrogel electrolytes, and ZnSO<sub>4</sub> provided the best results, benefiting from the Hofmeister salting-out effect. This effect improved hydrogen bonding between chains and hydrophobic effects, facilitating polymer cross-linking and toughening the hydrogel [99]. The gelatin ZnSO<sub>4</sub> hydrogel demonstrated a Young's modulus of 11.8 MPa, strength of about 1.5 MPa with a corresponding strain of over 120%, and ionic conductivity of 23.5 mS cm<sup>-1</sup> [99]. ZIBs utilizing this hydrogel electrolyte and a MnO<sub>2</sub> cathode achieved a specific capacity of 310 mAh g<sup>-1</sup> at a current density of 0.1 A g<sup>-1</sup> and a capacity retention of 67% after more than 9300 cycles at a current density of 2 A g<sup>-1</sup> (Figure 10) [99]. The ZIBs displayed a good electrode–electrolyte contact, as evidenced by small charge transfer impedance and diffusion impedance. The robust cycling stability indicated the absence of zinc dendrite formation [99]. Furthermore, the specific capacity remained unaffected after bending the ZIB 1000 times, attesting to the hydrogel's excellent mechanical properties [99].

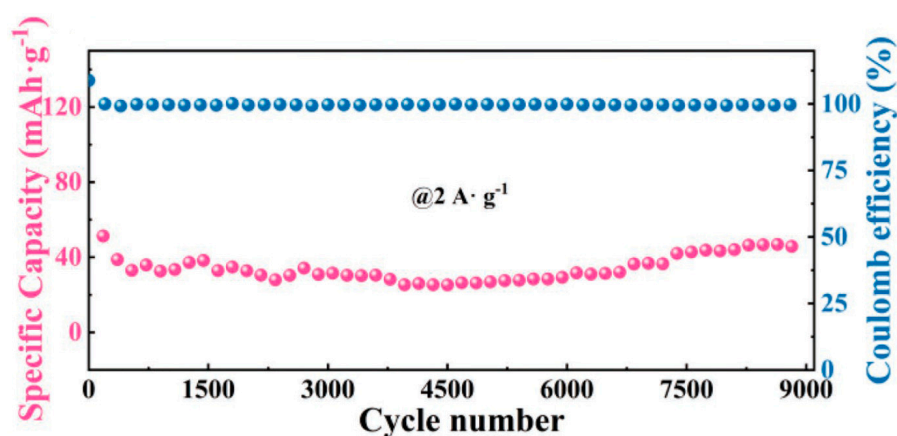


**Figure 10.** Long-term cycling performance, with specific capacity on the left axis and Coulombic efficiency on the right axis, for ZIB with gelatin-based hydrogel electrolyte and MnO<sub>2</sub> cathode at 2 A g<sup>-1</sup>. Figure slightly modified from [99] reprinted with permission.

#### 4.5. Xanthan Gum, Guar Gum, and Gum Arabic

Xanthan gum, a natural microbial polysaccharide, exhibits a primary structure comprising repeating pentasaccharide units consisting of two glucose units, two mannose units, and one glucuronic acid unit [121]. The main chain shares similarities with cellulose, featuring D-glucose units linked via  $\beta$ -1,4-glycosidic bonds [121]. Guar gum, extracted from the seeds of the plant *Cyamopsis tetragonoloba*, predominantly comprises galactomannans with linear chains of (1→4)-linked  $\beta$ -D-mannopyranosyl units and (1→6)-linked  $\alpha$ -D-galactopyranosyl residues as side chains [122]. Gum arabic, a complex polysaccharide with branched chains, can be neutral or slightly acidic, characterized by a backbone of 1,3-linked  $\beta$ -D-galactopyranosyl units and side chains of two to five 1,3-linked  $\beta$ -D-galactopyranosyl units connected to the backbone via 1,6-linkages [123].

Xanthan gum was employed to fabricate a stable sulfate-tolerant bio-electrolyte for ZIBs [124]. The electrolyte, prepared by dissolving 20 wt% xanthan gum powder in an aqueous solution of 2 M ZnSO<sub>4</sub> and 0.1 M MnSO<sub>4</sub> under stirring at room temperature, exhibited an ionic conductivity of 14.6 mS cm<sup>-1</sup> and displayed hydrating, adaptive, and adhesive behavior [124]. ZIBs utilizing this electrolyte and a MnO<sub>2</sub> cathode delivered a capacity of 260 mAh g<sup>-1</sup> at 1C, with 90% capacity retention and 100% Coulombic efficiency over 330 cycles at 1C [124]. Additionally, the ZIBs demonstrated durability under repeated bending and twisting [124].

In another study employing xanthan gum, a hydrogel was developed to enhance the performance of ZIBs at subzero temperatures [125]. In this case, the hydrogel electrolyte was prepared by mixing about 40 wt% xanthan gum powder in a 4 M ZnCl<sub>2</sub> aqueous solution under stirring at room temperature [125]. After adjusting the content and concentration of different components, the electrolyte exhibited an ionic conductivity of 6.26 mS/cm at 20 °C and 2.54 mS cm<sup>-1</sup> at -20 °C [125]. ZIBs with this electrolyte and a NH<sub>4</sub>V<sub>3</sub>O<sub>8</sub>·1.9H<sub>2</sub>O cathode delivered a capacity of 201 mAh g<sup>-1</sup> at a current density of 0.2 A g<sup>-1</sup> at -20 °C (Figure 11) [125]. Moreover, the ZIBs showed a cyclability with a capacity retention of 77% over 1500 cycles at a current density of 1.0 A g<sup>-1</sup> at -20 °C, and a capacity retention of 92% over 100 cycles while subjected to bending at -20 °C. The firm contact at the electrolyte–electrode interface remained stable at -20 °C [125].

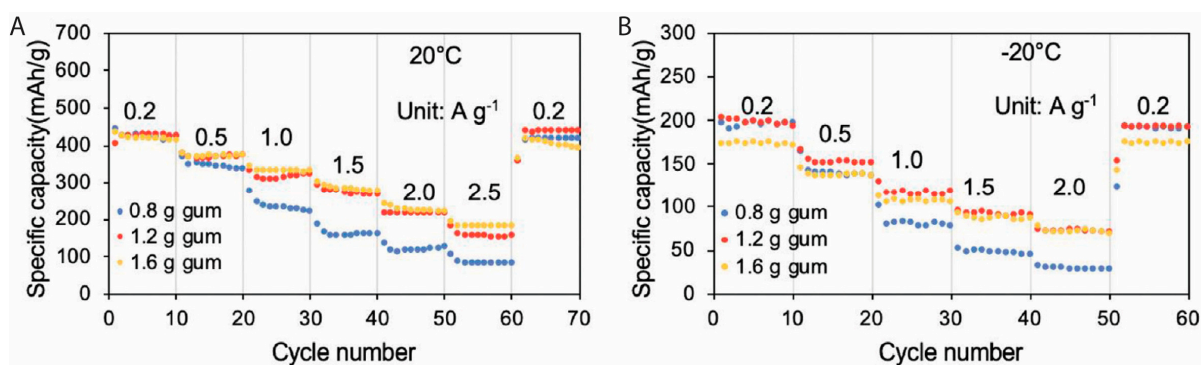


**Figure 11.** Rate performance of the ZIBs with xanthan gum hydrogel electrolyte for current densities ranging from 0.2 to 2.5 A g<sup>-1</sup> at 20 °C (A) and at -20 °C (B). Figure slightly modified from [125] reprinted with permission.

Guar gum was utilized to produce an electrolyte for flexible ZIBs with high rate performance and a long cycling life [126]. The hydrogel was made by dissolving 6 wt% guar gum in an aqueous solution of 2 M ZnSO<sub>4</sub> and 0.1 M MnSO<sub>4</sub> under stirring at room temperature [126]. The resulting hydrogel electrolyte exhibited an ionic conductivity of 10.7 mS cm<sup>-1</sup> at room temperature [126]. Thanks to its high ionic conductivity, ZIBs with this hydrogel electrolyte and an  $\alpha$ -MnO<sub>2</sub> cathode achieved the highest energy density of 416 Wh kg<sup>-1</sup> and a specific capacity of 308.2 mAh g<sup>-1</sup> at a current density of 0.3 A g<sup>-1</sup>, also demonstrating fast charging and discharging capabilities of 131.6 mAh g<sup>-1</sup> at a current density of 6.0 A g<sup>-1</sup> [126]. The ZIBs displayed very high cyclability with 100% capacity retention after 1900 cycles, and 85% capacity retention after 2000 cycles at a current density of 6.0 A g<sup>-1</sup>, indicating the positive effect of the hydrogel in suppressing zinc dendrite formation [126]. Moreover, the ZIBs exhibited good durability with respect to bending, showing a capacity retention of 81.3% after 1000-time bending [126].

Gum arabic was also employed to prepare a hydrogel electrolyte to suppress water-induced side reactions in ZIBs [127]. In this work, 30 wt% gum arabic was mixed in an aqueous solution of 1 M ZnSO<sub>4</sub> and 1 M Li<sub>2</sub>SO<sub>4</sub> under stirring at 80 °C for four minutes, followed by casting in a glass mold after another six minutes [127]. The abundant hydrogen bonding network suppressed the active water molecules and thus expanded the electrochemical window to up to 2.26 V. Measurements with Zn symmetric cells indicated a long lifetime of more than 1300 h for this gel electrolyte [127]. A Zn hybrid ion battery with this electrolyte and a LiFePO<sub>4</sub> cathode showed a Coulombic efficiency of 91.13% at 0.5C, indicating satisfactory ion migration between the cathode and anode, as well as controlled side reactions at the anode interface [127].

**Table 1.** Summary of all biopolymer hydrogel electrolytes for ZIBs with information on the type of biopolymer, electrolyte, mechanical strength, ionic conductivity, and main advantages and disadvantages.

Hydrogels [Ref.]	Electrolyte Salts	Mechanical Strength	Ionic Conductivity	Advantages	Disadvantages
Cellulose-based hydrogel [97]	3 M ZnSO <sub>4</sub>	39.5 MPa	0.643 mS cm <sup>-1</sup>	Low cost; Low thickness	Relatively low cycling stability; Low conductivity
Bacterial cellulose hydrogel [98]	2.0 M ZnSO <sub>4</sub> and 0.2 M MnSO <sub>4</sub>	~1.75 MPa	27.8 mS cm <sup>-1</sup>	Low cost; High stability; Easy fabrication	Relatively low mechanical properties
CMC hydrogel [53]	7 M KAc and 1 M ZnAc <sub>2</sub>	1.33 MPa	34.5 mS cm <sup>-1</sup>	Low cost; High cycling stability	Complex fabrication; Relatively low mechanical properties
Nanocellulose–CMC hydrogel [100]	2 M ZnSO <sub>4</sub>	70 MPa	26 mS cm <sup>-1</sup>	High cycling stability; Good rate performance; High tensile strength	Relatively complex fabrication
CMC with tetraethyl orthosilicate and glycerol [103]	4.5 M ZnSO <sub>4</sub>	2.11 MPa	19.4 mS cm <sup>-1</sup> @ -40 °C	Wide temperature stable window; Good stability	Relatively complex fabrication
Sorbitol-modified cellulose hydrogel electrolyte [52]	16 M ZnCl <sub>2</sub>	0.62 MPa	35.4 mS cm <sup>-1</sup>	Wide temperature stable window; High conductivity	Low mechanical strength; Relatively high cost
Chitosan-Zn membrane electrolyte [105]	2 M ZnSO <sub>4</sub>	7.4 MPa	71.8 mS cm <sup>-1</sup>	High conductivity; Non-flammability	Relatively complex fabrication
Natural chitosan-glass fiber hydrogel [106]	2 M ZnSO <sub>4</sub>	2.40 MPa	83.4 mS cm <sup>-1</sup>	Low cost; High conductivity	Glass fiber may limit the wearable application
Chitosan on cotton pad [107]	2 M ZnSO <sub>4</sub>	~5 MPa	-	Low cost; Dendrite control	Relatively low stability
Kappa (k)-carrageenan–chitosan hydrogel [109]	2 M ZnSO <sub>4</sub>	14.2 MPa	5.3 mS cm <sup>-1</sup>	High cycling stability; High mechanical strength	Low conductivity
Zinc alginate gel [112]	2 M ZnSO <sub>4</sub> and 0.2 M MnSO <sub>4</sub>	-	18.3 mS cm <sup>-1</sup>	Relatively high cycling stability	Relatively low temperature compatibility
Zinc alginate hydrogel [114]	2 M ZnSO <sub>4</sub>	4.63 MPa	0.54 mS cm <sup>-1</sup>	Self-healing; Easy fabrication	Low conductivity
Guar gum–alginate [116]	2 M ZnSO <sub>4</sub> and 0.1 M MnSO <sub>4</sub>	-	6.19 mS cm <sup>-1</sup> @ -20 °C	Wide temperature window	Unclear mechanical strength
Gelatin-based hydrogel electrolyte [60]	0.5 M Li <sub>2</sub> SO <sub>4</sub> and 0.5 M ZnSO <sub>4</sub>	~100 kPa	37.2 mS cm <sup>-1</sup>	High conductivity; Easy fabrication	Low mechanical strength
Gelatin hydrogel [99]	2 M ZnSO <sub>4</sub>	1.5 MPa	23.5 mS cm <sup>-1</sup>	Low material cost; High conductivity	Low mechanical strength; Relatively complex fabrication
Xanthan gum hydrogel [124]	2 M ZnSO <sub>4</sub> and 0.1 M MnSO <sub>4</sub>	-	14.6 mS cm <sup>-1</sup>	High conductivity; Easy fabrication	Low mechanical strength; Relatively low cycling stability
Xanthan gum hydrogel [125]	4 M ZnCl <sub>2</sub>	~0.1 MPa	2.54 mS cm <sup>-1</sup> @ -20 °C	Wide temperature stable window	Relatively low conductivity at room temperature; Low mechanical strength
Guar gum biopolymer electrolyte [126]	2 M ZnSO <sub>4</sub> and 0.1 M MnSO <sub>4</sub>	0.65 MPa	10.7 mS cm <sup>-1</sup>	Easy fabrication; Relatively high conductivity	Low mechanical strength

## 5. Hybrid Biopolymer–Synthetic Polymer Hydrogel Electrolytes for Zn-Ion Batteries

Biopolymers have been employed as a component in hybrid hydrogel electrolytes alongside synthetic polymers. This approach involves the formation of interpenetrating

network (IPN) hydrogels by two or more polymer networks. This strategy allows the synergistic properties of both polymers to be harnessed, such as achieving good mechanical strength and high water absorption capacity. Beyond considerations of biodegradability, the overall objectives of these electrolytes align with those of discussed biopolymer hydrogel electrolytes. These objectives include ensuring good mechanical strength and ionic conductivity, suppressing zinc dendrite formation and water-induced side reactions, and maintaining performance at subzero temperature. A summary of the investigated hybrid biopolymer-synthetic polymer hydrogel electrolytes for Zn-ion batteries with details on electrolyte type, mechanical strength, ionic conductivity and main advantages and disadvantages is presented in Table 2.

### 5.1. Cellulose and Its Derivatives with Synthetic Polymer

Multiple studies have explored double-network hydrogel electrolytes utilizing cellulose or cellulose derivatives and polyacrylamide (PAM) to develop flexible or stretchable ZIBs with high stability. For instance, a hydrogel electrolyte was devised using cellulose nanofibers and PAM [128]. The hydrogel was created by initially dispersing approximately 7 wt% cellulose nanofibers (of a 1.5 wt% water suspension) in an aqueous solution of 1 M  $\text{Zn}(\text{CF}_3\text{SO}_3)_2$  under stirring [128]. Subsequently, 0.2 wt% ammonium persulfate (APS), about 14 wt% acrylamide monomers, and 0.2 wt% *N,N'*-methylenebisacrylamide (NNMBA) were added to the solution. The solution was stirred at room temperature until casting, followed by heating in an oven at 60 °C to achieve free radical polymerization, with grafting of acrylamide onto the cellulose nanofibers [128]. ZIBs utilizing this hydrogel and a  $\text{Mg}_{0.23}\text{V}_2\text{O}_5 \cdot 1.0\text{H}_2\text{O}$  cathode demonstrated a specific capacity of 216 mAh g<sup>-1</sup> after 2000 cycles at a current density of 5 A g<sup>-1</sup>, with a capacity retention of 98.6% [128]. The ZIBs remained operational even at a strain of 650%, under repeated bending, heating, and freezing conditions [128]. Recently, lignin-containing cellulose nanofibers and PAM were employed to create a double-network, water-retaining hydrogel electrolyte for dendrite-free ZIBs [129]. For this hydrogel electrolyte, 10 mM  $\text{Zn}(\text{OTf})_2$ , 33 wt% acrylamide, 0.4 wt% APS, and 0.04 wt% NNMBA cross-linker were added to a lignin-containing cellulose nanofiber suspension under stirring [129]. The solution was then poured into a mold and heated at 60 °C for polymerization [129]. ZIBs with this hydrogel electrolyte and a MgVO cathode exhibited a specific capacity of 320 mAh g<sup>-1</sup>, with a capacity retention of 91.9% after 4000 cycles at a current density of 0.2 A g<sup>-1</sup> [129]. The entangled dual-network structure, coupled with strong hydrogen bonding with lignin-containing cellulose nanofibers, effectively limited water molecules, contributing to outstanding stability. These ZIBs maintained an energy density of 255.4 Wh kg<sup>-1</sup> at a power density of 341.7 W kg<sup>-1</sup> for over 5000 cycles, with a voltage window from 0.2 V to 1.9 V [129].

Apart from cellulose nanofibers, cellulose derivatives have been employed to produce double-network structured hydrogel electrolytes. For instance, a CMC-PAM hydrogel electrolyte was developed for flexible ZIBs to enhance mechanical properties and suppress zinc dendrite formation [130]. To prepare the hydrogel, CMC and acrylamide monomer were dissolved in deionized water under stirring [130]. For in situ polymerization, potassium persulfate (PPS) was added as an initiator, and NNMBA was added as a cross-linker. The solution was cast and heated at 80 °C [130]. Subsequently, the produced hydrogel was immersed in an aqueous solution of 2 M  $\text{ZnSO}_4$  and 0.1 M  $\text{MnSO}_4$  [130]. The hydrogel's double-network structure with intermolecular interactions improved the electrolyte's toughness through energy dissipation during deformation. Simultaneously, the negatively charged carboxyl groups in the hydrogel trapped zinc ions, facilitating homogeneous zinc deposition on the anode, promoting reversibility and stability [130]. The hydrogel achieved a maximum stretchability of 3000% strain with recovery to 800%, and full original shape recovery up to 400% stretching [130]. An ionic conductivity of 13 mS cm<sup>-1</sup> was determined for this electrolyte at room temperature [130]. ZIBs with this electrolyte and an  $\alpha\text{-MnO}_2$  cathode delivered a specific capacity of 245.4  $\mu\text{Ah cm}^{-2}$  at 0.154 mA cm<sup>-2</sup> and a capacity

retention of 90.2% over 500 cycles at  $0.308 \text{ mA cm}^{-2}$  [130]. Moreover, the ZIBs exhibited good endurance under bending and mechanical impact [130].

In another study, an amphoteric double-network hydrogel electrolyte was developed using carboxyethyl quaternized cellulose, PAM, and  $\text{ZnSO}_4$  (Figure 12) to create highly stable ZIBs [131]. The intermolecular interactions, coordination bonds, and covalent cross-linking provided both strength and toughness. ZIBs with this hydrogel electrolyte and a  $\text{NH}_4\text{V}_4\text{O}_{10}$  cathode demonstrated a specific capacity of  $299 \text{ mAh g}^{-1}$  at a current density of  $0.5 \text{ A g}^{-1}$ , with a capacity retention of 92% after 200 cycles and a Coulombic efficiency of more than 99.9% [131]. At a current density of  $2 \text{ A g}^{-1}$ , the ZIBs delivered a capacity of  $195 \text{ mA g}^{-1}$  after 2000 cycles, corresponding to a capacity retention of 86% [131]. A hydrogel was also developed by cross-linking hydroxyethyl cellulose with divinyl sulfone in the presence of CMC [132]. In this work, CMC and hydroxyethyl cellulose were dissolved in a KOH solution of pH 12 to 13 under stirring, and then divinyl sulfone was added and stirred until a gel was obtained [132]. The introduction of CMC improved water retention through its high affinity with water, and the  $\text{Na}^+$  ions from CMC also provided more free ions, contributing to good ionic conductivity of 5 to  $6 \text{ mS cm}^{-1}$  [132]. For use as the electrolyte in ZIBs, the hydrogel was immersed in an aqueous solution of  $1 \text{ M ZnCl}_2$ , and in a printed ZIB with this electrolyte and a  $\text{MnO}_2$  cathode, a capacity of  $11 \text{ mAh g}^{-1}$  was measured at a current density of  $0.5 \text{ A g}^{-1}$  [132].

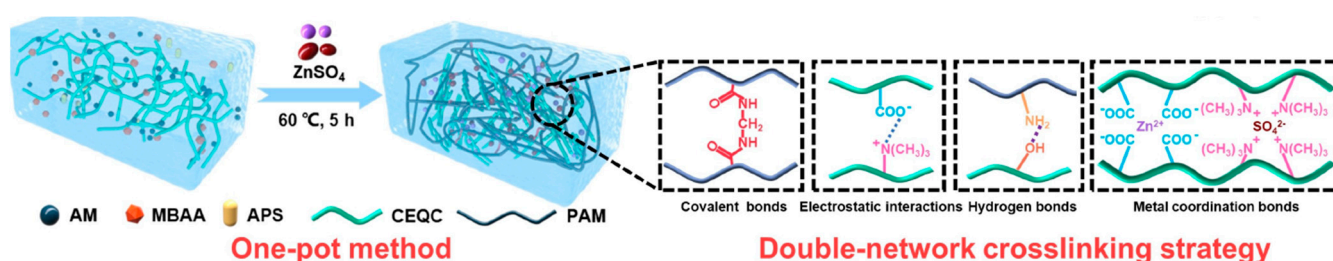


**Figure 12.** Schematic diagram displaying the synthesis of the amphoteric double-network hydrogel with carboxyethyl quaternized cellulose (CEQC), PAM, and  $\text{ZnSO}_4$ , and the interactions in the hydrogel, including covalent bonds, electrostatic interactions, hydrogen bonds, and metal coordination bonds. Figure slightly modified from [131] reprinted with permission.

In addition, triple interpenetrating network hydrogel electrolytes were developed for ZIBs with extended stability. For instance, a hydrogel electrolyte was formulated using CMC, gelatin, and PAM [133]. To prepare the hydrogel, 2 wt% CMC and 2 to 18 wt% gelatin were dissolved in an aqueous solution of  $2 \text{ M ZnSO}_4$  and  $0.1 \text{ M MnSO}_4$  under stirring at  $50 \text{ }^\circ\text{C}$  [133]. This solution was then combined with another solution obtained by dissolving  $3 \text{ M}$  acrylamide and  $0.1 \text{ wt}\%$  NNMBA in an aqueous solution of  $2 \text{ M ZnSO}_4$  and  $0.1 \text{ M MnSO}_4$  under stirring at room temperature [133]. Subsequently,  $0.2 \text{ wt}\%$  PPS was added to the mixture, followed by heating at  $70 \text{ }^\circ\text{C}$  for one hour under a vacuum, resulting in the hydrogel electrolyte [133]. The hydrogel electrolyte, exhibiting reversible hydrogen bonding interactions and entanglement, could maintain its structure during deformation by dissipating energy and restore mechanical strength later. The triple interpenetrating network also provided a high water affinity and water retention. The hydrogel exhibited an ionic conductivity of  $27.0 \text{ mS cm}^{-1}$ , tensile strength of  $108.3 \text{ kPa}$ , and elongation at break of  $1014\%$ . It maintained mechanical stability even at a temperature of  $-20 \text{ }^\circ\text{C}$  (Figure 13A–C) [133]. ZIBs with this hydrogel electrolyte and a HMgVO cathode delivered a capacity of  $368.9 \text{ mAh g}^{-1}$  at a current density of  $0.1 \text{ A g}^{-1}$  [133]. Moreover, the ZIBs exhibited good cycling stability for 10,000 cycles at  $0 \text{ }^\circ\text{C}$  with a capacity of  $51.6 \text{ mAh g}^{-1}$  at a current density of  $10 \text{ A g}^{-1}$  and a capacity retention of 72.7% (Figure 13D) [133].

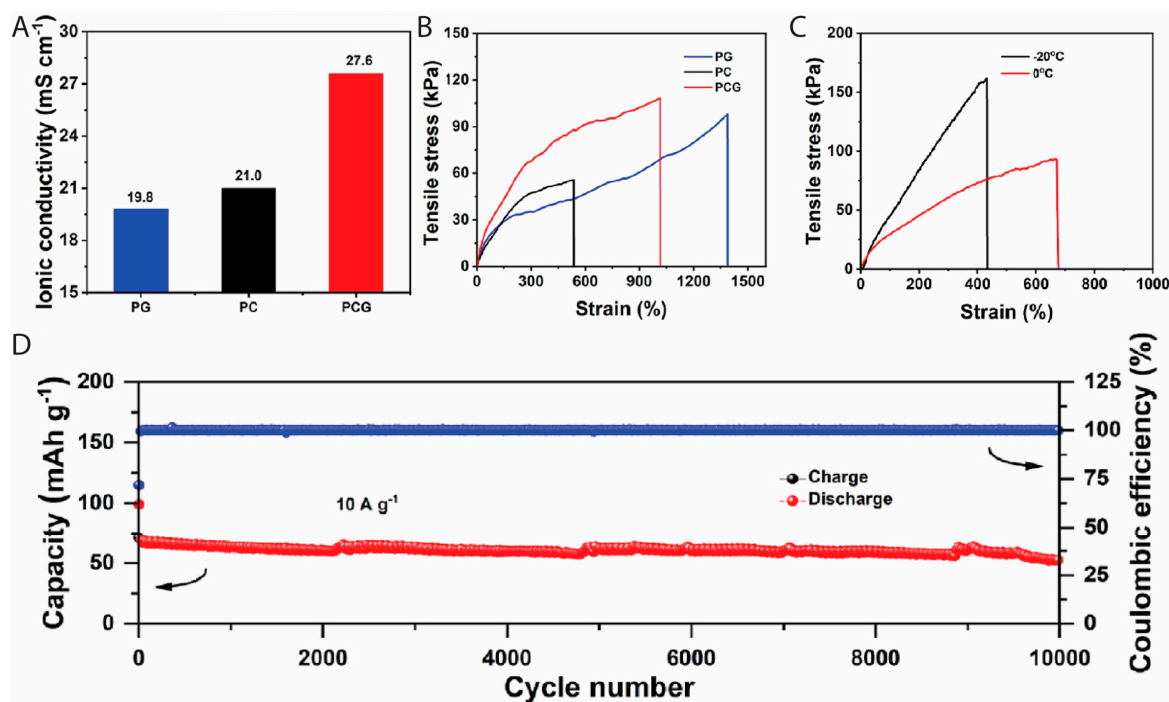


**Figure 13.** (A) Ionic conductivity for the PAM-gelatin (PG), PAM-CMC (PC), and PAM-CMC-gelatin (PCG) hydrogel electrolytes. (B) Stress–strain plot for the PAM-gelatin (PG), PAM-CMC (PC), and PAM-CMC-gelatin (PCG) hydrogel electrolytes. (C) Stress–strain plot for the PAM-CMC-gelatin hydrogel electrolyte at 0 and at  $-20^{\circ}\text{C}$ . (D) Long-term cycling performance at  $0^{\circ}\text{C}$  at a current density of  $10\text{ A g}^{-1}$ . Figure slightly modified from [133] reprinted with permission.

In another study, a PAM-poly(ethylene glycol) diacrylate-CMC hydrogel electrolyte was developed [134]. The hydrogel was prepared by dissolving acrylamide, CMC, and poly(ethylene glycol) diacrylate in a  $2\text{ M ZnSO}_4$  aqueous solution, followed by heating at  $40^{\circ}\text{C}$  [134]. The ionic conductivity of the hydrogel electrolyte was  $30.24\text{ mS cm}^{-1}$  [134]. Moreover, the amide groups in PAM molecules demonstrated a significant influence on reducing the desolvation activation energy; specifically, the strong bonding between  $\text{Zn}^{2+}$  and amide inhibited the formation of a solvation sheath and promoted an even zinc ion distribution. ZIBs with this electrolyte and a  $\text{V}_2\text{O}_5 \cdot 1.6\text{H}_2\text{O}$  cathode delivered a specific capacity of  $381\text{ mAh g}^{-1}$  at a current density of  $1.0\text{ A g}^{-1}$ , with a capacity retention rate of 71.1% [134].

Some other efforts regarding hybrid cellulose–synthetic polymer hydrogel electrolytes focused on ZIBs operating at extremely cold temperatures. For example, a cellulose nanofiber-PAM hydrogel electrolyte with a hybrid methanol/water solvent was developed [135]. The hydrogel was prepared by dissolving acrylamide monomers, APS, and NNMBA in deionized water, followed by adding cellulose nanofibers under stirring at  $25^{\circ}\text{C}$ . Then, the solution was cast and heated at  $60^{\circ}\text{C}$  [135]. The hydrogel membrane was immersed in the hybrid aqueous solution with an optimized methanol molar ratio of 56% and about 40 wt%  $\text{Zn}(\text{CF}_3\text{SO}_3)_2$  [135]. ZIBs with this hydrogel electrolyte and a  $\text{MgVO}$  cathode delivered a specific capacity of  $214\text{ mAh g}^{-1}$  after 4000 cycles at  $10\text{ A g}^{-1}$  [135]. The ZIBs exhibited high flexibility with repeated bending and twisting even at a very cold temperature. The hydrogen bonding between methanol molecular clusters and water molecules effectively reduced the freezing point. The ZIBs delivered a capacity of more than  $130\text{ mAh g}^{-1}$  at a current density of  $0.01\text{ A g}^{-1}$  at a temperature of  $-60^{\circ}\text{C}$  [135].

In another study focusing on ZIBs with anti-freezing capability, glycerol was employed in the preparation process [136]. Initially, nanocellulose was extracted from wheat straws through grinding and ball-milling, followed by treatment with  $\text{NaOH}$ ,  $\text{H}_2\text{O}_2$ , and UV light radiation [136]. After freeze-drying, the nanocellulose powder was utilized to produce films

by dispersing it in water through stirring and sonification, followed by subsequent vacuum filtration and drying [136]. Despite the applied treatment not fully removing the lignin, the extracted cellulose-based material exhibited commendable mechanical properties and stability in water [136]. To prepare the electrolyte, the nanocellulose material was dispersed in water, and acrylamide and glycerol were added to the solution under stirring, followed by sonification, casting, and heating at 60 °C [136]. As a final step, the hydrogel film was immersed in an aqueous solution of 2 M ZnSO<sub>4</sub> and 0.2 M MnSO<sub>4</sub> [136]. By utilizing such an electrolyte as a physical reinforcer in the cathode and electrolyte, the ZIBs with MnO<sub>2</sub> active materials achieved a capacity of 309.2 mAh g<sup>-1</sup> at 0.2 A g<sup>-1</sup> and a capacity retention of 85.2% after 1000 cycles, and demonstrated excellent anti-freezing ability and durability under mechanical deformation [136].

Multifunctional systems were also developed. For instance, a multifunctional flexible ZIB was created with a stable thermochromic hydrogel, based on CMC IV, cotton cellulose nanofibers, and PAM, enabling a high-temperature warning functionality [137]. The hydrogel synthesis procedure can be summarized as follows: First, 15 wt% cellulose nanofibers were added to deionized water, followed by the addition of 1 M ZnSO<sub>4</sub>·7H<sub>2</sub>O under stirring [137]. Subsequently, 12 wt% acrylamide and 0.5 wt% CMC were added to the solution under stirring, and then 0.2 wt% TCCP, 0.2 wt% APS initiator, and 0.06 wt% NNMBA cross-linking agent were added [137]. After five hours of stirring and degassing, the solution was cast and heated to 50 °C for 12 h of curing [137]. The hydrogel demonstrated excellent thermochromic features when subjected to cycling between 25 and 60 °C, attributed to the even dispersion of the colorant and developer by CNF and CMC. ZIBs with this electrolyte delivered a capacity of 383 mAh g<sup>-1</sup> at a current density of 0.5 A g<sup>-1</sup>, with a capacity retention of 98% after 1000 cycles and 81% after 3500 cycles [137].

In another study, a ZIB-type self-powered strain sensing system was developed with an ionic hydrogel made from CMC, PAM, and tannic acid [138]. The hydrogel electrolyte was prepared by first adding 1 w/v% CMC, 1 w/v% tannic acid, 27 w/v% acrylamide, 0.02 w/v% NNMBA, and 0.0004 vol% photoinitiator to an aqueous solution of 2 M ZnSO<sub>4</sub> and 0.1 M MnSO<sub>4</sub> under stirring [138]. This was followed by degassing and transfer to a mold, after which it was exposed to ultraviolet light irradiation at room temperature [138]. The tannic acid induced the formation of sites with multiple interactions, which could be used for energy dissipation and achieve good mechanical properties. The hydrogel had a tensile strength of 132 kPa and strain of 622%, and it exhibited self-healing and adhesive properties [138]. ZIBs with this hydrogel electrolyte and a MnO<sub>2</sub> cathode delivered a specific capacity of 223.0 mAh g<sup>-1</sup> at a current density of 1.0 A g<sup>-1</sup>, showing a capacity retention of 79.6% after 500 cycles at a current density of 5.0 A g<sup>-1</sup> [138].

## 5.2. Chitosan, Chitin, or Derivatives with Synthetic Polymer

For the development of a chemically self-charging flexible ZIB, a hydrogel electrolyte was produced from chitin and PAM [139]. To create the hydrogel, the authors initially generated a 1 wt% chitin nanofiber suspension through a combined deep eutectic solvent and high-pressure homogenization treatment on raw lobster shells [139]. Subsequently, 0.01 M Zn(CF<sub>3</sub>SO<sub>3</sub>)<sub>2</sub> was dissolved in the chitin nanofiber suspension [139]. Free radical polymerization was then employed by adding 33 wt% acrylamide monomers, 0.4 wt% APS, and 0.02 wt% NNMBA to the solution under stirring at room temperature, followed by casting and heating at 60 °C [139]. ZIBs utilizing this electrolyte and a VO<sub>2</sub> cathode achieved a specific capacity of 343.9 mAh g<sup>-1</sup> at a current density of 0.2 A g<sup>-1</sup> (Figure 14), along with an energy density of 231.9 Wh kg<sup>-1</sup> at a power density of 139.0 W kg<sup>-1</sup> [139]. The ZIBs in this study exhibited dual operation modes, allowing both chemical and galvanostatic charging hybrid modes [139]. Remarkably, the cathodes could self-charge by reacting with oxygen, and the exposure to air was highly accessible due to the unique design and the use of hydrogel electrolytes. The ZIBs demonstrated a discharging capacity of 263.9 mAh g<sup>-1</sup> at a current density of 0.2 A g<sup>-1</sup> after 6 h of oxidation in air [139]. A total of 20 cycles of

galvanostatic discharging and chemical self-charging were achieved by adding acetic acid to the hydrogel electrolyte to remove the byproduct  $Zn_x(OTf)_y(OH)_{2x-y} \cdot nH_2O$  [139].

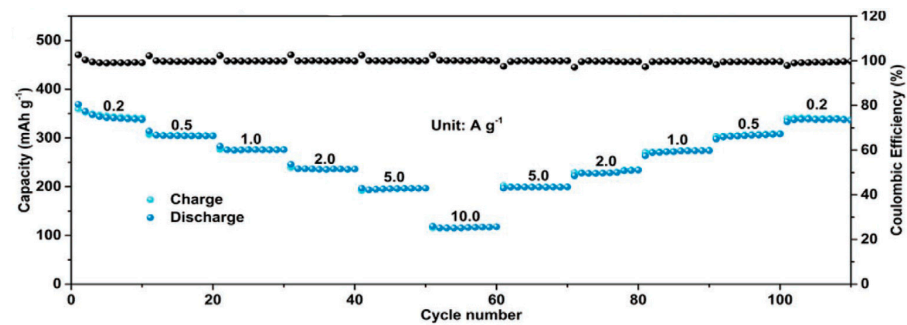


**Figure 14.** Rate performance, with capacity (blue symbols) on the left axis and Coulombic efficiency (black symbols) on the right axis, of the ZIB with chitin-PAM hydrogel electrolyte and  $VO_2$  cathode for current densities ranging from 0.2 to  $10 \text{ A g}^{-1}$ . Figure slightly modified from [139] reprinted with permission.

In another study, a soaking-free and self-healing hydrogel electrolyte for ZIBs was developed using chitosan and PAM [71]. The hydrogel was prepared by dissolving chitosan in a 1.25 vol% acetic acid solution, followed by the addition of zinc tribuoromethanesulfonate, acrylamide, MBAA, and APS under stirring [71]. This mixture was then poured into a mold and heated at  $60 \text{ }^\circ\text{C}$  to polymerize the hydrogel electrolyte [71]. Coin cell ZIBs with this hydrogel electrolyte and polyaniline cathode exhibited a specific capacity of  $172 \text{ mAh g}^{-1}$  and maintained 94.6% of capacity after 2000 cycles at a current density of  $3 \text{ A g}^{-1}$  [71]. Pouch cell ZIBs with these components delivered stable energy even in severe conditions of bending, pressing, piercing, and hammering [71].

A multifunctional hydrogel was developed with carboxymethyl chitosan, PAM, and LiCl (Figure 15) to create a rechargeable ZIB for flexible, self-powered integrated sensing systems [140]. Carboxymethyl chitosan was dissolved in an aqueous solution of  $2 \text{ M ZnSO}_4$  and  $0.1 \text{ M MnSO}_4$  [140]. Subsequently, an acrylamide monomer,  $\text{LiCl} \cdot \text{H}_2\text{O}$ , and a photoinitiator were added to the solution under stirring, followed by transfer to a mold and ultraviolet light irradiation [140]. The produced hydrogel had an ionic conductivity of  $5.6 \text{ mS cm}^{-1}$ , a tensile strength of  $67 \text{ kPa}$ , a strain of 640%, self-healing ability, and anti-drying and anti-freezing ( $-48 \text{ }^\circ\text{C}$ ) properties [140]. It is worth noting that sufficient non-covalent bonding inside the hydrogel network endowed the electrolyte with a self-healing function via its reversibility. ZIBs with this hydrogel electrolyte and an  $\alpha\text{-MnO}_2$  cathode delivered a specific capacity of  $214.2 \text{ mAh g}^{-1}$  at a current density of  $0.5 \text{ A g}^{-1}$ , with a capacity retention of 75% after 500 cycles at  $4.0 \text{ A g}^{-1}$ , and an 88.3% electrochemical performance retention after being cut [140].

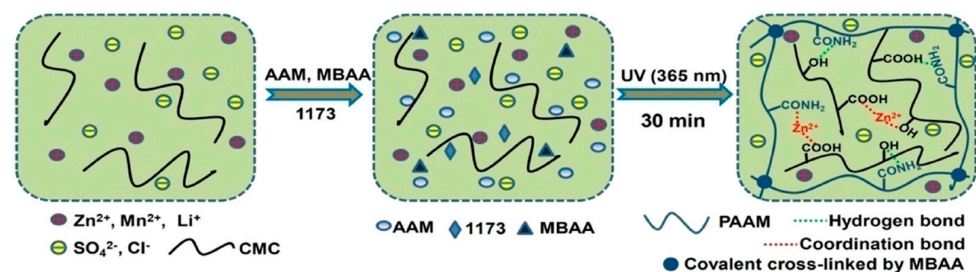


**Figure 15.** Schematic diagram illustrating the preparation method of the PAM-chitosan-LiCl hydrogel with addition of acrylamide monomers (AAMs) and MBAA photoinitiator to the carboxymethyl chitosan (CMC) solution, followed by an ultraviolet irradiation (UV) step. Figure from [140] reprinted with permission.

### 5.3. Alginate with Synthetic Polymer

To enhance the stability of ZIBs and mitigate cathode dissolution, a hydrogel based on sodium alginate and PAM was developed for ZIBs with a  $\text{Na}^+$  preintercalated  $\delta\text{-Na}_{0.65}\text{Mn}_2\text{O}_4 \cdot 1.31\text{H}_2\text{O}$  cathode [141]. The hydrogel was formed by dissolving sodium alginate in deionized water under stirring at room temperature, followed by the addition of the acrylamide monomer. Subsequently, NNMBA was introduced as a cross-linker, APS as a photoinitiator, and  $N,N,N',N'$ -tetramethylethylenediamine (TMEDA) as a cross-linker accelerator for PAM formation [141]. The PAM film was cured at  $50\text{ }^\circ\text{C}$  and then immersed in an aqueous solution of  $1\text{ M ZnSO}_4$  and  $0.2\text{ M MnSO}_4$  to create the hydrogel electrolyte [141]. The preintercalated sodium ions supported the layered  $\text{MnO}_2$  structure, further enhancing stability. The resulting ZIB delivered a capacity of  $305\text{ mAh g}^{-1}$  at  $0.1\text{ A g}^{-1}$ , exhibited excellent Coulombic efficiency of over 99%, and maintained capacity retention of 96% for 1000 cycles at  $2\text{ A g}^{-1}$  [141].

### 5.4. Gelatin with Synthetic Polymer

A zwitterionic triple-network hydrogel electrolyte with robust tensile and compressive strength was developed for flexible textile-based ZIBs [142]. The hydrogel was composed of PAM, gelatin, and [2-(methylacryloxy) ethyl] dimethyl-(3-sulfonic acid propyl) ammonium hydroxide (DMAPS) [142]. Initially, acrylamide, DMAPS, 1-carrageenan, and NNMBA were dissolved in deionized water at  $60\text{ }^\circ\text{C}$ . TMEDA and PPS initiator were added, and the mixture was further stirred at  $60\text{ }^\circ\text{C}$  [142]. Subsequently, the hydrogel was refrigerated at  $4\text{ }^\circ\text{C}$  [142]. The ionic conductivity of this hydrogel electrolyte was  $35.1\text{ mS cm}^{-1}$  [142], owing to the zwitterionic groups on DMAPS that promoted the migration of both cations and anions. ZIBs with this electrolyte and a  $\delta\text{-MnO}_2$  cathode delivered a stable capacity of  $175\text{ mAh g}^{-1}$  for 100 cycles at a current density of  $0.4\text{ A g}^{-1}$ , with a Coulombic efficiency of over 99%. The ZIBs remained operational under bending or mechanical pressure [142].

### 5.5. Xanthan Gum with Synthetic Polymer

To create flexible ZIBs for submarine use, a stable hydrogel electrolyte was developed based on a mixture of xanthan gum, PAM, and cotton cellulose nanofibers (Figure 16) [143]. Radical polymerization was applied to make the hydrogel, starting with dissolving 10 wt% acrylamide and 0.5 wt% xanthan gum powder in an aqueous cotton cellulose nanofiber dispersion under stirring at room temperature. The addition of  $(\text{NH}_4)_2\text{S}_2\text{O}_8$  as an initiator and NNMBA as a cross-linker followed under stirring [143]. After a vacuum treatment, the solution was cast at  $65\text{ }^\circ\text{C}$  to remove bubbles [143]. Subsequently, the hydrogel film was immersed in an aqueous solution of  $2\text{ M ZnSO}_4$  and  $0.1\text{ M MnSO}_4$  to make the electrolyte [143]. The high molecular weight and numerous side-chain groups on xanthan gum created strong interactions between ions and water, forming a stable hydrogel network. The strong ion adsorption provided high stability underwater. ZIBs with this electrolyte and a  $\text{MnO}_2$  cathode delivered a specific capacity of  $237\text{ mAh g}^{-1}$  at 1C, with a capacity retention of 86.2% after 1000 cycles at 4C [143]. Moreover, after bending the ZIB for 500 times, a capacity retention of 94.5% was achieved, and immersing the ZIB in water for two hours led to a capacity retention of 85.1% [143].

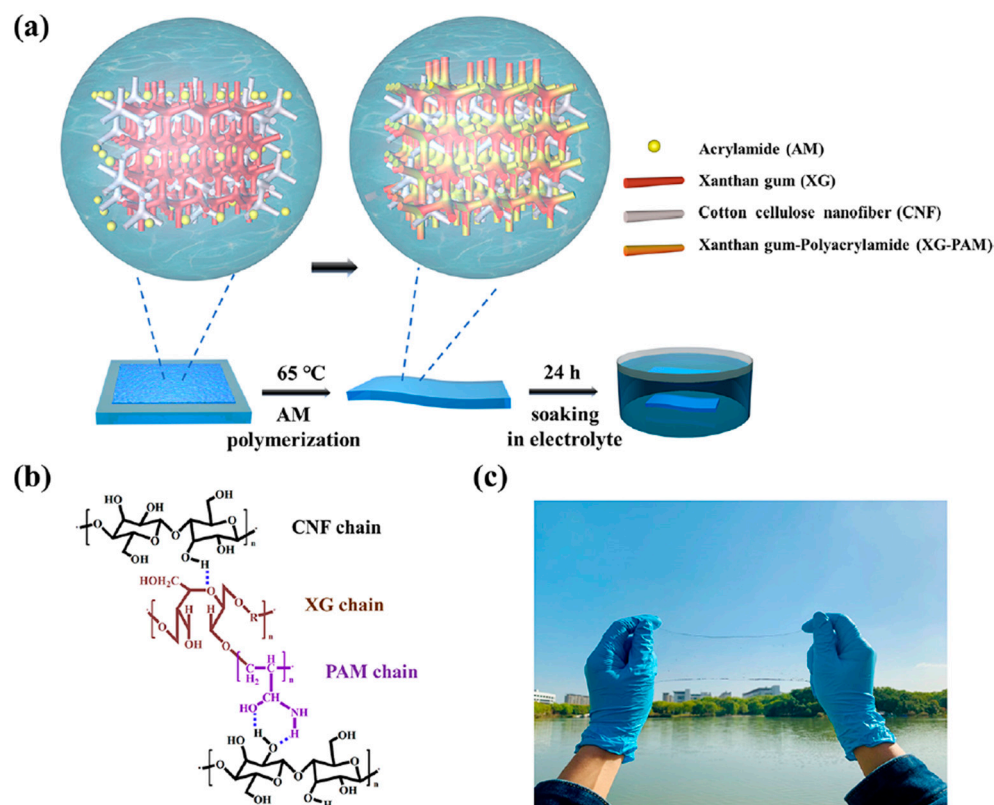


**Figure 16.** (a) Schematic diagram of the preparation method to produce xanthan gum-PAM-cellulose nanofiber hydrogel with polymerization and electrolyte immersion steps. (b) Chemical structure of the hydrogel with cellulose nanofibers (CNFs), xanthan gum (XG), and polyacrylamide (PAM) chains. (c) Photograph of the hydrogel. Figure from [143] reprinted with permission.

### 5.6. Agar with Synthetic Polymer

Agar, a natural polysaccharide extracted from certain marine red algae, comprises a blend of agarpectin (non-gelling) and agarose (gelling) [144]. Agarose is a linear polysaccharide with repeating units of D-galactose and 3,6-anhydro-L-galactose, connected by alternating  $\alpha$ -(1 $\rightarrow$ 3) and  $\beta$ -(1 $\rightarrow$ 4) glycosidic bonds [144]. Agarose has a gelling temperature of approximately 30–40 °C and a melting temperature of 80–90 °C, and is soluble in warm water and some organic solvents [145]. A hydrogel electrolyte based on agar and PAM was developed for ZIBs with the goal of expanding the operational temperature range [146]. The hydrogel was prepared by dissolving agar and PAM in a 5:1 weight ratio in ultrapure water under stirring and heating, followed by casting and heating at 60 °C [146]. Subsequently, the hydrogel films were vacuum-dried at 80 °C [146]. The hydrogel electrolyte was obtained by immersing the hydrogel film in a 3 M ZnSO<sub>4</sub> aqueous solution with 30 wt% ethylene glycol [146]. Agar hydroxyl and amide groups facilitated preferable Zn<sup>2+</sup> transfer, paving the way for high conductivity and minimal polarization. ZIBs with this hydrogel electrolyte and a V<sub>2</sub>O<sub>5</sub> cathode delivered a capacity of 315 mAh g<sup>-1</sup> at a current density of 0.1 A g<sup>-1</sup>, and the ZIBs exhibited stable cycling at temperatures ranging from -25 °C to 50 °C [146].

### 5.7. Soybean Protein with Synthetic Polymer

Soybean protein and PAM were employed to fabricate a highly compressible electrolyte for flexible ZIBs [147]. The hydrogel was prepared by dispersing 3.3 wt% soybean protein isolate nanoparticles in deionized water under stirring and a nitrogen atmosphere at 95 °C, followed by cooling. Acrylamide monomers, 2-hydroxy-4-(2-hydroxyethoxy)-2-methylpropiophenone as a photoinitiator, and NNMBA as a cross-linker were then added [147]. The solution was poured into a Teflon mold, subjected to ultraviolet light

irradiation for five hours, and dried overnight at 60 °C. Subsequently, the hydrogel was immersed in an aqueous solution of 1 M ZnSO<sub>4</sub> and 0.1 M MnSO<sub>4</sub> to obtain the hydrogel electrolyte [147]. The negatively charged soybean protein increased the dielectric constant and enhanced electrochemical performance. ZIBs with this hydrogel electrolyte and a MnO<sub>2</sub> cathode delivered a specific capacity of 299.3 mAh g<sup>-1</sup> at a current density of 0.4C, with a capacity retention rate of 78.2% over 500 cycles (Figure 17). Furthermore, the ZIBs maintained performance even under bending and hammering conditions [147].

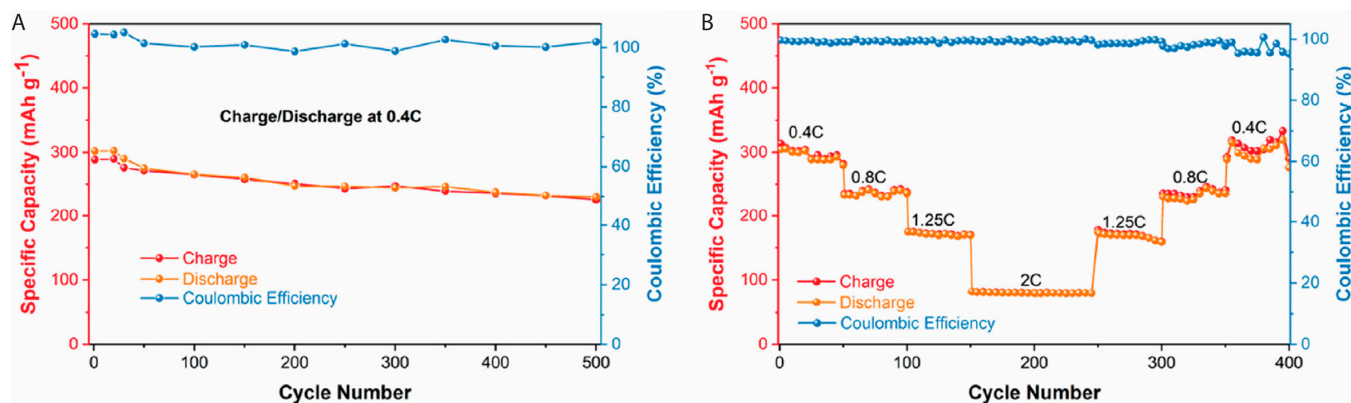


**Figure 17.** (A) Cycling performance of ZIB with PAM-soybean protein hydrogel electrolyte at a current density of 0.4C. The capacity retention rate is 78.2% over 500 cycles. (B) Rate performance of ZIB with PAM-soybean protein hydrogel electrolyte for current densities ranging from 0.4 to 2C. Both graphs display specific capacity on the left axis and Coulombic efficiency on the right axis. Figure slightly modified from [147] reprinted with permission.

**Table 2.** Summary of all discussed hybrid biopolymer–synthetic polymer hydrogel electrolytes for ZIBs with information on the type of biopolymer, electrolyte, mechanical strength, ionic conductivity, and main advantages and disadvantages.

Hydrogels [Ref.]	Electrolyte Salts	Mechanical Strength	Ionic Conductivity	Advantages	Disadvantages
Cellulose nanofiber–PAM hydrogel electrolyte [128]	1 M Zn(CF <sub>3</sub> SO <sub>3</sub> ) <sub>2</sub>	192 kPa	6.8 mS cm <sup>-1</sup>	High cycling stability; Wide temperature stable window	Low mechanical strength; Complex fabrication
Lignin-containing cellulose nanofiber–PAM hydrogel [129]	1 M Zn(OTf) <sub>2</sub>	350 kPa	21.57 mS cm <sup>-1</sup>	High cycling stability; Dendrite growth control	Low mechanical strength; Relatively expensive salts
CMC–PAM hydrogel electrolyte [130]	2 M ZnSO <sub>4</sub> and 0.1 M MnSO <sub>4</sub>	~35 kPa	13 mS cm <sup>-1</sup>	High stretchability; Relatively low cost	Low mechanical strength
PAM/CMC/gelatin hydrogel electrolyte [133]	2 M ZnSO <sub>4</sub> and 0.1 M MnSO <sub>4</sub>	108.3 kPa	27.0 mS cm <sup>-1</sup>	High conductivity; Wide temperature stable window	Low mechanical strength; Complex fabrication
PAM–poly(ethylene glycol) diacrylate–CMC hydrogel [134]	2 M ZnSO <sub>4</sub>	2.25 MPa	30.24 mS cm <sup>-1</sup>	High conductivity; High mechanical strength	Relatively low cycling stability
Cellulose nanofiber–PAM hydrogel [135]	40 wt% Zn(CF <sub>3</sub> SO <sub>3</sub> ) <sub>2</sub>	~250 kPa	-	Wide temperature stable window; High cycling stability	Relatively low mechanical strength
PAM–cotton cellulose nanofiber–CMC hydrogel [137]	1 M ZnSO <sub>4</sub>	60 kPa	2.492 S m <sup>-1</sup>	Very high conductivity; High stretchability	Low mechanical strength
PAM–chitin nanofiber hydrogel [139]	0.01 M Zn(CF <sub>3</sub> SO <sub>3</sub> ) <sub>2</sub>	114.62 kPa	15.2 mS cm <sup>-1</sup>	High cycling stability	Low mechanical strength; Relatively expensive electrolyte salt

Table 2. Cont.

Hydrogels [Ref.]	Electrolyte Salts	Mechanical Strength	Ionic Conductivity	Advantages	Disadvantages
Carboxymethyl chitosan-PAM hydrogel [140]	2 M ZnSO <sub>4</sub> and 0.1 M MnSO <sub>4</sub>	67 kPa	5.6 mS cm <sup>-1</sup>	Low conductivity and mechanical strength	Reliable anti-freezing (-48 °C) feature
Alginate-PAM hydrogel [141]	1 M ZnSO <sub>4</sub> and 0.2 M MnSO <sub>4</sub>	~500 kPa	29.2 mS cm <sup>-1</sup>	High conductivity	Relatively complex fabrication
PAM-gelatin-DMAPS hydrogel [142]	2 M ZnSO <sub>4</sub>	~35 kPa	35.1 mS cm <sup>-1</sup>	High conductivity	Low mechanical strength
Xanthan gum-PAM-cotton cellulose nanofibers [143]	2 M ZnSO <sub>4</sub> and 0.1 M MnSO <sub>4</sub>	84 kPa	28.8 mS cm <sup>-1</sup>	Water proofing; Stability under deformation	Low mechanical strength
Agar-PAM hydrogel [146]	3 M ZnSO <sub>4</sub>	92.34 MPa	-	High mechanical strength; Dendrite growth control; Anti-freezing feature	Relatively low conductivity
Soybean protein-PAM hydrogel [147]	1 M ZnSO <sub>4</sub> and 0.1 M MnSO <sub>4</sub>	31.3 KPa	50.8 mS cm <sup>-1</sup>	Relatively high conductivity; High stability under deformation	Low mechanical strength

## 6. Future Perspectives

The impressive performance exhibited by biopolymer hydrogel electrolytes is accelerating the development of next-generation ZIB applications. Biopolymer hydrogels, primarily derived from natural polymers sourced from animals and plants, are characterized by the ability of polysaccharides and proteins to form gel networks with water molecules. These networks involve intermolecular interactions that facilitate gelation, augmented by the presence of multiple hydrophilic groups in the chain structures [148].

In the realm of flexible ZIBs, the merits of biopolymer hydrogels have become evident. Firstly, their water-included feature and 3D network structures confer suitable mechanical strength and reliable ionic conductivity, making them desirable for battery applications. The flexibility and toughness of hydrogels also impart higher structural integrity and durability to ZIBs under harsh mechanical deformation. Secondly, biomaterials are ideal for ZIBs due to their easy obtainability, low cost, environmental friendliness, and high biocompatibility. Notably, transient devices for wearable, implantable, and sustainable power supply applications have been developed using biocompatible gels such as agarose (patent US10655024B2) and gelatin-silk protein [149].

Moreover, extensive opportunities for further modification arise from the plethora of biopolymer hydrogels. For instance, grafting or cross-linking with synthetic hydrogel polymers enhances mechanical strength and ionic conductivity. Additionally, in-depth research on hybrid biopolymer electrolytes has led to the development of functions such as anti-freezing, water retention, and self-healing, expanding their applicability across various scenarios. The functional groups within biopolymers play a crucial role in improving zinc ion transfer and regulating the interfacial chemical environment, ensuring the stable and efficient operation of ZIBs.

Despite these achievements, challenges persist with hydrogel electrolytes for ZIBs, prompting further attention and exploration in specific areas:

1. First of all, the design of ionic conductivity and mechanical properties of the hydrogel electrolyte is still in need of further optimization. The relatively larger thickness of a hydrogel electrolyte, compared to a liquid electrolyte, as well as the lower water content, inevitably reduce conductivity. In this context, additional research into double-network and triple-network hydrogels could be conducted. Such interpenetrating network structures can enhance mechanical strength, durability, and robustness. Moreover, ionic conductivity can be increased by developing polymer networks with a higher number of hydrophilic groups on their chains, improving water retention. In-

terpenetrating network structures can be further explored for hydrogel electrolytes in ZIBs using multiple biopolymers rather than hybrid biopolymers–synthetic polymers to make the hydrogels greener and more cost-effective, such as further study around relatively rigid CMC and other highly conductive polysaccharides.

2. Moreover, further design efforts could focus more on the mechanical properties and electrochemical performance on the entire ZIB cell. Ensuring the firm integration of electrodes with the electrolyte and maintaining stability during large, long-term deformation are essential for the lifespan of ZIBs. Interfaces should also be enhanced to achieve a more stable environment for various interfacial reactions. Simple modifications on the electrode side (such as the addition of non-covalent interactions), and even the integration of electrodes with hydrogel electrolytes, might expand the electrochemical stable window to a higher level or offer better interfacial contact during deformation. Fundamental research focused on understanding interfacial mechanisms, combining DFT calculations, computer simulations, and experimental research involving in operando characterization can provide better insights and help improve the future design and development of hydrogel electrolytes in ZIBs.
3. Apart from stability during deformation, durability under harsh environments undeniably impacts the performance of ZIBs. Certain conditions, such as temperature variations, bending, and other deformations, may lead to the aging of hydrogels, including shrinkage, reduction in adhesion, and decreased wettability, all resulting in increased interface resistance and deteriorating efficiency at the electrode–electrolyte interface [91]. Thus, water retention capability still needs further investigation to improve conductivity stability throughout the lifespan, potentially expanding application scenes to low-temperature and large-scale energy storage, offshore energy storage, and smart wearable electronics.
4. In addition, better strategies need to be developed for widening the electrochemical stable window for hydrogel ZIBs, as the current additives used may influence the ionic conductivity of the hydrogel or affect aqueous interactions at the interface. The subtle utilization of different polar groups, controlling free water molecules, and using charged or zwitterionic groups to regulate ionic movement may be effective choices for controlling side reactions. However, the use of functional groups or specific polymers may also result in a change in electrochemical performance, and a detailed investigation of compatibility between different components should be performed.
5. The development of biopolymer electrolytes also needs more attention regarding the possibility of commercialization. Although the high natural abundance of most biopolymers theoretically improves accessibility, some hydrogels may not be competitive enough compared to mature aqueous systems, limited by their relatively small markets and high prices. Moreover, the synthesis of hybrid electrolytes could introduce complicated processes or high-cost materials, leading to an increase in expenses. More efforts can be dedicated to making modifications based on low-price raw materials, such as CMC, alginate, starch, etc., among biobased hydrogels, as well as synthetic materials with stable and economical supplies, such as PAM and PVA. It is gratifying that increasing applications and patents focusing on ZIBs with hydrogel electrolytes have been launched in recent years, with many exploring the future of biopolymer electrolytes (e.g., CN113644227A; EP4078716A1; US20180166662A1; WO2022197984A1).
6. The next generation of battery assembly will pave the way for extensive applications of ZIBs with biohydrogels. Compared to conventional cells, 3D-printed ZIBs have already demonstrated multiple advantages, such as miniaturization, flexibility, customization, and high safety. Very recently, polyacrylamide–hemicellulose/EGaIn microdroplet hydrogel has been successfully applied as hydrogel ink for 3D-printed ZIBs [150]. Similarly, PAM-based cross-linked hydrogel electrolytes have also demonstrated their potential in 3D-printing ZIBs [151]. Utilizing the features of biopolymer hydrogels for further improvement in areal capacity and stability of electrodes, as well

as the related development for wearable or even implantable practical applications, will propel the potential usage of ZIBs.

**Author Contributions:** Conceptualization, V.V. and J.W.; validation, V.V. and J.W.; investigation, V.V. and J.W.; writing—original draft preparation, V.V.; writing—review and editing, V.V. and J.W.; visualization, V.V. and J.W.; supervision, V.V.; project administration, V.V.; funding acquisition, V.V. and J.W. All authors have read and agreed to the published version of the manuscript.

**Funding:** This research was funded by FWO (Fonds Wetenschappelijk Onderzoek), strategic basic research PhD fellowship, grant number: 1SHI624N.

**Data Availability Statement:** No new data were produced in this work. The original data can be found in the cited publications.

**Acknowledgments:** We acknowledge funding by FWO.

**Conflicts of Interest:** The authors declare no conflicts of interest.

## References

1. Kang, M.J.; Hwang, Y.C. Exploring the Factors Affecting the Continued Usage Intention of IoT-Based Healthcare Wearable Devices Using the TAM Model. *Sustainability* **2022**, *14*, 12492. [[CrossRef](#)]
2. Ding, Y.L.; Cano, Z.P.; Yu, A.P.; Lu, J.; Chen, Z.W. Automotive Li-Ion Batteries: Current Status and Future Perspectives. *Electrochem. Energy Rev.* **2019**, *2*, 1–28. [[CrossRef](#)]
3. Dunn, B.; Kamath, H.; Tarascon, J.M. Electrical Energy Storage for the Grid: A Battery of Choices. *Science* **2011**, *334*, 928–935. [[CrossRef](#)] [[PubMed](#)]
4. Fang, X.; Ge, M.Y.; Rong, J.P.; Zhou, C.W. Free-Standing LiNi<sub>0.5</sub>Mn<sub>1.5</sub>O<sub>4</sub>/Carbon Nanofiber Network Film as Lightweight and High-Power Cathode for Lithium Ion Batteries. *ACS Nano* **2014**, *8*, 4876–4882. [[CrossRef](#)] [[PubMed](#)]
5. Yan, P.F.; Zheng, J.M.; Liu, J.; Wang, B.Q.; Cheng, X.P.; Zhang, Y.F.; Sun, X.L.; Wang, C.M.; Zhang, J.G. Tailoring grain boundary structures and chemistry of Ni-rich layered cathodes for enhanced cycle stability of lithium-ion batteries. *Nat. Energy* **2018**, *3*, 600–605. [[CrossRef](#)]
6. Bresser, D.; Hosoi, K.; Howell, D.; Li, H.; Zeisel, H.; Amine, K.; Passerini, S. Perspectives of automotive battery R&D in China, Germany, Japan, and the USA. *J. Power Sources* **2018**, *382*, 176–178. [[CrossRef](#)]
7. Fang, G.Z.; Zhou, J.; Pan, A.Q.; Liang, S.Q. Recent Advances in Aqueous Zinc-Ion Batteries. *ACS Energy Lett.* **2018**, *3*, 2480–2501. [[CrossRef](#)]
8. Golmohammadzadeh, R.; Faraji, F.; Jong, B.; Pozo-Gonzalo, C.; Banerjee, P.C. Current challenges and future opportunities toward recycling of spent lithium-ion batteries. *Renew. Sustain. Energy Rev.* **2022**, *159*, 112202. [[CrossRef](#)]
9. Baird, A.R.; Archibald, E.J.; Marr, K.C.; Ezekoye, O.A. Explosion hazards from lithium-ion battery vent gas. *J. Power Sources* **2020**, *446*, 227257. [[CrossRef](#)]
10. Xie, X.S.; Li, J.J.; Xing, Z.Y.; Lu, B.A.; Liang, S.Q.; Zhou, J. Biocompatible zinc battery with programmable electro-cross-linked electrolyte. *Natl. Sci. Rev.* **2023**, *10*, nwac281. [[CrossRef](#)]
11. Li, J.; Wang, X.D. Materials Perspectives for Self-Powered Cardiac Implantable Electronic Devices toward Clinical Translation. *Acc. Mater. Res.* **2021**, *2*, 739–750. [[CrossRef](#)]
12. Li, J.J.; Ruan, P.C.; Chen, X.H.; Lei, S.R.; Lu, B.A.; Chen, Z.Z.; Zhou, J. Aqueous Batteries for Human Body Electronic Devices Focus Review. *ACS Energy Lett.* **2023**, *8*, 2904–2918. [[CrossRef](#)]
13. Duan, J.J.; Xie, W.K.; Yang, P.H.; Li, J.; Xue, G.B.; Chen, Q.; Yu, B.Y.; Liu, R.; Zhou, J. Tough hydrogel diodes with tunable interfacial adhesion for safe and durable wearable batteries. *Nano Energy* **2018**, *48*, 569–574. [[CrossRef](#)]
14. Hwang, J.Y.; Myung, S.T.; Sun, Y.K. Sodium-ion batteries: Present and future. *Chem. Soc. Rev.* **2017**, *46*, 3529–3614. [[CrossRef](#)] [[PubMed](#)]
15. Slater, M.D.; Kim, D.; Lee, E.; Johnson, C.S. Sodium-Ion Batteries. *Adv. Funct. Mater.* **2013**, *23*, 947–958. [[CrossRef](#)]
16. Yabuuchi, N.; Kubota, K.; Dahbi, M.; Komaba, S. Research Development on Sodium-Ion Batteries. *Chem. Rev.* **2014**, *114*, 11636–11682. [[CrossRef](#)]
17. Pramudita, J.C.; Sehwat, D.; Goonetilleke, D.; Sharma, N. An Initial Review of the Status of Electrode Materials for Potassium-Ion Batteries. *Adv. Energy Mater.* **2017**, *7*, 1602911. [[CrossRef](#)]
18. Zhang, W.C.; Liu, Y.J.; Guo, Z.P. Approaching high-performance potassium-ion batteries via advanced design strategies and engineering. *Sci. Adv.* **2019**, *5*, eaav7412. [[CrossRef](#)]
19. Rajagopalan, R.; Tang, Y.G.; Ji, X.B.; Jia, C.K.; Wang, H.Y. Advancements and Challenges in Potassium Ion Batteries: A Comprehensive Review. *Adv. Funct. Mater.* **2020**, *30*, 1909486. [[CrossRef](#)]

20. Huie, M.M.; Bock, D.C.; Takeuchi, E.S.; Marschilok, A.C.; Takeuchi, K.J. Cathode materials for magnesium and magnesium-ion based batteries. *Coord. Chem. Rev.* **2015**, *287*, 15–27. [[CrossRef](#)]
21. Wang, F.; Fan, X.L.; Gao, T.; Sun, W.; Ma, Z.H.; Yang, C.Y.; Han, F.; Xu, K.; Wang, C.S. High-Voltage Aqueous Magnesium Ion Batteries. *ACS Cent. Sci.* **2017**, *3*, 1121–1128. [[CrossRef](#)] [[PubMed](#)]
22. Gummow, R.J.; Vamvounis, G.; Kannan, M.B.; He, Y.H. Calcium-Ion Batteries: Current State-of-the-Art and Future Perspectives. *Adv. Mater.* **2018**, *30*, 1801702. [[CrossRef](#)] [[PubMed](#)]
23. Park, J.; Xu, Z.L.; Yoon, G.; Park, S.K.; Wang, J.; Hyun, H.; Park, H.; Lim, J.; Ko, Y.J.; Yun, Y.S.; et al. Stable and High-Power Calcium-Ion Batteries Enabled by Calcium Intercalation into Graphite. *Adv. Mater.* **2020**, *32*, 1904411. [[CrossRef](#)] [[PubMed](#)]
24. Wang, M.; Jiang, C.L.; Zhang, S.Q.; Song, X.H.; Tang, Y.B.; Cheng, H.M. Reversible calcium alloying enables a practical room-temperature rechargeable calcium-ion battery with a high discharge voltage. *Nat. Chem.* **2018**, *10*, 667–672. [[CrossRef](#)] [[PubMed](#)]
25. Zhang, N.; Chen, X.Y.; Yu, M.; Niu, Z.Q.; Cheng, F.Y.; Chen, J. Materials chemistry for rechargeable zinc-ion batteries. *Chem. Soc. Rev.* **2020**, *49*, 4203–4219. [[CrossRef](#)] [[PubMed](#)]
26. Tang, B.Y.; Shan, L.T.; Liang, S.Q.; Zhou, J. Issues and opportunities facing aqueous zinc-ion batteries. *Energy Environ. Sci.* **2019**, *12*, 3288–3304. [[CrossRef](#)]
27. Konarov, A.; Voronina, N.; Jo, J.H.; Bakenov, Z.; Sun, Y.K.; Myung, S.T. Present and Future Perspective on Electrode Materials for Rechargeable Zinc-Ion Batteries. *ACS Energy Lett.* **2018**, *3*, 2620–2640. [[CrossRef](#)]
28. Das, S.K.; Mahapatra, S.; Lahan, H. Aluminium-ion batteries: Developments and challenges. *J. Mater. Chem. A* **2017**, *5*, 6347–6367. [[CrossRef](#)]
29. Lin, M.C.; Gong, M.; Lu, B.G.; Wu, Y.P.; Wang, D.Y.; Guan, M.Y.; Angell, M.; Chen, C.X.; Yang, J.; Hwang, B.J.; et al. An ultrafast rechargeable aluminium-ion battery. *Nature* **2015**, *520*, 324–328. [[CrossRef](#)]
30. Wang, D.Y.; Wei, C.Y.; Lin, M.C.; Pan, C.J.; Chou, H.L.; Chen, H.A.; Gong, M.; Wu, Y.P.; Yuan, C.Z.; Angell, M.; et al. Advanced rechargeable aluminium ion battery with a high-quality natural graphite cathode. *Nat. Commun.* **2017**, *8*, 14283. [[CrossRef](#)]
31. Zhang, Y.; Liu, S.Q.; Ji, Y.J.; Ma, J.M.; Yu, H.J. Emerging Nonaqueous Aluminium-Ion Batteries: Challenges, Status, and Perspectives. *Adv. Mater.* **2018**, *30*, 1706310. [[CrossRef](#)] [[PubMed](#)]
32. Kundu, D.; Vajargah, S.H.; Wan, L.W.; Adams, B.; Prendergast, D.; Nazar, L.F. Aqueous vs. nonaqueous Zn-ion batteries: Consequences of the desolvation penalty at the interface. *Energy Environ. Sci.* **2018**, *11*, 881–892. [[CrossRef](#)]
33. Liu, S.; Kang, L.; Kim, J.M.; Chun, Y.T.; Zhang, J.; Jun, S.C. Recent Advances in Vanadium-Based Aqueous Rechargeable Zinc-Ion Batteries. *Adv. Energy Mater.* **2020**, *10*, 2000477. [[CrossRef](#)]
34. Jia, X.X.; Liu, C.F.; Neale, Z.G.; Yang, J.H.; Cao, G.Z. Active Materials for Aqueous Zinc Ion Batteries: Synthesis, Crystal Structure, Morphology, and Electrochemistry. *Chem. Rev.* **2020**, *120*, 7795–7866. [[CrossRef](#)]
35. Wan, F.; Niu, Z.Q. Design Strategies for Vanadium-based Aqueous Zinc-Ion Batteries. *Angew. Chem.-Int. Ed.* **2019**, *58*, 16358–16367. [[CrossRef](#)]
36. Zhu, X.D.; Cao, Z.Y.; Wang, W.J.; Li, H.J.; Dong, J.C.; Gao, S.P.; Xu, D.X.; Li, L.; Shen, J.F.; Ye, M.X. Superior-Performance Aqueous Zinc-Ion Batteries Based on the In Situ Growth of MnO<sub>2</sub> Nanosheets on V<sub>2</sub>CTX MXene. *ACS Nano* **2021**, *15*, 2971–2983. [[CrossRef](#)] [[PubMed](#)]
37. Yang, Q.; Li, Q.; Liu, Z.X.; Wang, D.H.; Guo, Y.; Li, X.L.; Tang, Y.C.; Li, H.F.; Dong, B.B.; Zhi, C.Y. Dendrites in Zn-Based Batteries. *Adv. Mater.* **2020**, *32*, 2001854. [[CrossRef](#)]
38. Zhang, Q.; Luan, J.Y.; Tang, Y.G.; Ji, X.B.; Wang, H.Y. Interfacial Design of Dendrite-Free Zinc Anodes for Aqueous Zinc-Ion Batteries. *Angew. Chem.-Int. Ed.* **2020**, *59*, 13180–13191. [[CrossRef](#)]
39. Cao, Z.Y.; Zhuang, P.Y.; Zhang, X.; Ye, M.X.; Shen, J.F.; Ajayan, P.M. Strategies for Dendrite-Free Anode in Aqueous Rechargeable Zinc Ion Batteries. *Adv. Energy Mater.* **2020**, *10*, 2001599. [[CrossRef](#)]
40. Cao, J.; Zhang, D.D.; Zhang, X.Y.; Zeng, Z.Y.; Qin, J.Q.; Huang, Y.H. Strategies of regulating Zn<sup>2+</sup> solvation structures for dendrite-free and side reaction-suppressed zinc-ion batteries. *Energy Environ. Sci.* **2022**, *15*, 499–528. [[CrossRef](#)]
41. Wu, B.K.; Zhang, G.B.; Yan, M.Y.; Xiong, T.F.; He, P.; He, L.; Xu, X.; Mai, L.Q. Graphene Scroll-Coated  $\alpha$ -MnO<sub>2</sub> Nanowires as High-Performance Cathode Materials for Aqueous Zn-Ion Battery. *Small* **2018**, *14*, 1703850. [[CrossRef](#)] [[PubMed](#)]
42. Liu, S.L.; Mao, J.F.; Pang, W.K.; Vongsvivut, J.; Zeng, X.H.; Thomsen, L.; Wang, Y.Y.; Liu, J.W.; Li, D.; Guo, Z.P. Tuning the Electrolyte Solvation Structure to Suppress Cathode Dissolution, Water Reactivity, and Zn Dendrite Growth in Zinc-Ion Batteries. *Adv. Funct. Mater.* **2021**, *31*, 2104281. [[CrossRef](#)]
43. Zhang, D.D.; Cao, J.; Zhang, X.Y.; Insin, N.; Wang, S.M.; Han, J.T.; Zhao, Y.S.; Qin, J.Q.; Huang, Y.H. Inhibition of Manganese Dissolution in Mn<sub>2</sub>O<sub>3</sub> Cathode with Controllable Ni<sup>2+</sup> Incorporation for High-Performance Zinc Ion Battery. *Adv. Funct. Mater.* **2021**, *31*, 2009412. [[CrossRef](#)]
44. Bayaguud, A.; Fu, Y.P.; Zhu, C.B. Interfacial parasitic reactions of zinc anodes in zinc ion batteries: Underestimated corrosion and hydrogen evolution reactions and their suppression strategies. *J. Energy Chem.* **2022**, *64*, 246–262. [[CrossRef](#)]
45. Cai, Y.; Chua, R.; Srinivasan, M. Anode Materials for Rechargeable Aqueous Al-Ion Batteries: Progress and Prospects. *Chem-nanomater* **2022**, *8*, e202100507. [[CrossRef](#)]
46. Lv, Y.Q.; Xiao, Y.; Ma, L.T.; Zhi, C.Y.; Chen, S.M. Recent Advances in Electrolytes for “Beyond Aqueous” Zinc-Ion Batteries. *Adv. Mater.* **2022**, *34*, 2106409. [[CrossRef](#)] [[PubMed](#)]

47. Liu, D.; Tang, Z.H.; Luo, L.F.; Yang, W.L.; Liu, Y.; Shen, Z.H.; Fan, X.H. Self-Healing Solid Polymer Electrolyte with High Ion Conductivity and Super Stretchability for All-Solid Zinc-Ion Batteries. *ACS Appl. Mater. Interfaces* **2021**, *13*, 36320–36329. [[CrossRef](#)]
48. Zeng, Y.X.; Zhang, X.Y.; Meng, Y.; Yu, M.H.; Yi, J.N.; Wu, Y.Q.; Lu, X.H.; Tong, Y.X. Achieving Ultrahigh Energy Density and Long Durability in a Flexible Rechargeable Quasi-Solid-State Zn-MnO<sub>2</sub> Battery. *Adv. Mater.* **2017**, *29*, 1700274. [[CrossRef](#)]
49. Zhao, J.W.; Sonigara, K.K.; Li, J.J.; Zhang, J.; Chen, B.B.; Zhang, J.J.; Soni, S.S.; Zhou, X.H.; Cui, G.L.; Chen, L.Q. A Smart Flexible Zinc Battery with Cooling Recovery Ability. *Angew. Chem.-Int. Ed.* **2017**, *56*, 7871–7875. [[CrossRef](#)]
50. Deng, Y.Q.; Wu, Y.H.; Wang, L.L.; Zhang, K.F.; Wang, Y.; Yan, L.F. Polysaccharide hydrogel electrolytes with robust interfacial contact to electrodes for quasi-solid state flexible aqueous zinc ion batteries with efficient suppressing of dendrite growth. *J. Colloid Interface Sci.* **2023**, *633*, 142–154. [[CrossRef](#)]
51. Guo, Y.Q.; Lim, G.J.H.; Verma, V.; Cai, Y.; Chua, R.; Lim, J.J.N.; Srinivasan, M. Solid State Zinc and Aluminum ion batteries: Challenges and Opportunities. *Chemsuschem* **2023**, *16*, e202202297. [[CrossRef](#)] [[PubMed](#)]
52. Quan, Y.H.; Zhou, W.J.; Wu, T.; Chen, M.F.; Han, X.; Tian, Q.H.; Xu, J.L.; Chen, J.Z. Sorbitol-modified cellulose hydrogel electrolyte derived from wheat straws towards high-performance environmentally adaptive flexible zinc-ion batteries. *Chem. Eng. J.* **2022**, *446*, 137056. [[CrossRef](#)]
53. Quan, Y.H.; Ma, H.; Chen, M.F.; Zhou, W.J.; Tian, Q.H.; Han, X.; Chen, J.Z. Salting-Out Effect Realizing High-Strength and Dendrite-Inhibiting Cellulose Hydrogel Electrolyte for Durable Aqueous Zinc-Ion Batteries. *ACS Appl. Mater. Interfaces* **2023**, *15*, 44974–44983. [[CrossRef](#)]
54. Wang, X.L.; Wang, B.; Cheng, J.L. Multi-Healable, Mechanically Durable Double Cross-Linked Polyacrylamide Electrolyte Incorporating Hydrophobic Interactions for Dendrite-Free Flexible Zinc-Ion Batteries. *Adv. Funct. Mater.* **2023**, *33*, 2304470. [[CrossRef](#)]
55. Xia, H.; Xu, G.; Cao, X.; Miao, C.Y.; Zhang, H.N.; Chen, P.Y.; Zhou, Y.; Zhang, W.; Sun, Z.M. Single-Ion-Conducting Hydrogel Electrolytes Based on Slide-Ring Pseudo-Polyrotaxane for Ultralong-Cycling Flexible Zinc-Ion Batteries. *Adv. Mater.* **2023**, *35*, e2301996. [[CrossRef](#)] [[PubMed](#)]
56. Chan, C.Y.; Wang, Z.Q.; Jia, H.; Ng, P.F.; Chow, L.; Fei, B. Recent advances of hydrogel electrolytes in flexible energy storage devices. *J. Mater. Chem. A* **2021**, *9*, 2043–2069. [[CrossRef](#)]
57. Leng, K.T.; Li, G.J.; Guo, J.J.; Zhang, X.Y.; Wang, A.X.; Liu, X.J.; Luo, J.Y. A Safe Polyzwitterionic Hydrogel Electrolyte for Long-Life Quasi-Solid State Zinc Metal Batteries. *Adv. Funct. Mater.* **2020**, *30*, 2001317. [[CrossRef](#)]
58. Chen, G.Q.; Huang, J.R.; Gu, J.F.; Peng, S.J.; Xiang, X.T.; Chen, K.; Yang, X.X.; Guan, L.H.; Jiang, X.C.; Hou, L.X. Highly tough supramolecular double network hydrogel electrolytes for an artificial flexible and low-temperature tolerant sensor. *J. Mater. Chem. A* **2020**, *8*, 6776–6784. [[CrossRef](#)]
59. Ma, R.J.; Xu, Z.X.; Wang, X.L. Polymer Hydrogel Electrolytes for Flexible and Multifunctional Zinc-Ion Batteries and Capacitors. *Energy Environ. Mater.* **2023**, *6*, e12464. [[CrossRef](#)]
60. Han, Q.; Chi, X.W.; Zhang, S.M.; Liu, Y.Z.; Zhou, B.A.; Yang, J.H.; Liu, Y. Durable, flexible self-standing hydrogel electrolytes enabling high-safety rechargeable solid-state zinc metal batteries. *J. Mater. Chem. A* **2018**, *6*, 23046–23054. [[CrossRef](#)]
61. Xu, T.; Liu, K.; Sheng, N.; Zhang, M.H.; Liu, W.; Liu, H.Y.; Dai, L.; Zhang, X.Y.; Si, C.L.; Du, H.S.; et al. Biopolymer-based hydrogel electrolytes for advanced energy storage/conversion devices: Properties, applications, and perspectives. *Energy Storage Mater.* **2022**, *48*, 244–262. [[CrossRef](#)]
62. Wang, Z.F.; Li, H.F.; Tang, Z.J.; Liu, Z.X.; Ruan, Z.H.; Ma, L.T.; Yang, Q.; Wang, D.H.; Zhi, C.Y. Hydrogel Electrolytes for Flexible Aqueous Energy Storage Devices. *Adv. Funct. Mater.* **2018**, *28*, 1804560. [[CrossRef](#)]
63. Liu, Y.; Zhou, H.; Zhou, W.X.; Meng, S.; Qi, C.; Liu, Z.; Kong, T.T. Biocompatible, High-Performance, Wet-Adhesive, Stretchable All-Hydrogel Supercapacitor Implant Based on PANI@rGO/Mxenes Electrode and Hydrogel Electrolyte. *Adv. Energy Mater.* **2021**, *11*, 2101329. [[CrossRef](#)]
64. Mo, F.N.; Chen, Z.; Liang, G.J.; Wang, D.H.; Zhao, Y.W.; Li, H.F.; Dong, B.B.; Zhi, C.Y. Zwitterionic Sulfobetaine Hydrogel Electrolyte Building Separated Positive/Negative Ion Migration Channels for Aqueous Zn-MnO<sub>2</sub> Batteries with Superior Rate Capabilities. *Adv. Energy Mater.* **2020**, *10*, 2000035. [[CrossRef](#)]
65. Li, J.; Yu, P.F.; Zhang, S.T.; Wen, Z.L.; Wen, Y.H.; Zhou, W.Y.; Dong, X.M.; Liu, Y.L.; Liang, Y.R. Mild synthesis of superadhesive hydrogel electrolyte with low interfacial resistance and enhanced ionic conductivity for flexible zinc ion battery. *J. Colloid Interface Sci.* **2021**, *600*, 586–593. [[CrossRef](#)] [[PubMed](#)]
66. Owusu, K.A.; Pan, X.; Yu, R.; Qu, L.; Liu, Z.; Wang, Z.; Tahir, M.; Haider, W.A.; Zhou, L.; Mai, L. Introducing Na<sub>2</sub>SO<sub>4</sub> in aqueous ZnSO<sub>4</sub> electrolyte realizes superior electrochemical performance in zinc-ion hybrid capacitor. *Mater. Today Energy* **2020**, *18*, 100529. [[CrossRef](#)]
67. Liu, C.X.; Xie, X.S.; Lu, B.G.; Zhou, J.; Liang, S.Q. Electrolyte Strategies toward Better Zinc-Ion Batteries. *ACS Energy Lett.* **2021**, *6*, 1015–1033. [[CrossRef](#)]
68. Wang, Y.B.; Li, Q.; Hong, H.; Yang, S.; Zhang, R.; Wang, X.Q.; Jin, X.; Xiong, B.; Bai, S.C.; Zhi, C.Y. Lean-water hydrogel electrolyte for zinc ion batteries. *Nat. Commun.* **2023**, *14*, 3890. [[CrossRef](#)]
69. Xu, P.J.; Wang, C.Y.; Zhao, B.X.; Zhou, Y.; Cheng, H.F. A high-strength and ultra-stable halloysite nanotubes-crosslinked polyacrylamide hydrogel electrolyte for flexible zinc-ion batteries. *J. Power Sources* **2021**, *506*, 230196. [[CrossRef](#)]

70. Yan, Y.C.; Duan, S.D.; Liu, B.; Wu, S.W.; Alsaied, Y.; Yao, B.W.; Nandi, S.; Du, Y.J.; Wang, T.W.; Li, Y.Z.; et al. Tough Hydrogel Electrolytes for Anti-Freezing Zinc-Ion Batteries. *Adv. Mater.* **2023**, *35*, 230196. [[CrossRef](#)]
71. Liu, Y.Q.; Gao, A.M.; Hao, J.N.; Li, X.L.; Ling, J.Z.; Yi, F.Y.; Li, Q.Z.; Shu, D. Soaking-free and self-healing hydrogel for wearable zinc-ion batteries. *Chem. Eng. J.* **2023**, *452*, 139605. [[CrossRef](#)]
72. Ni, Q.; Kim, B.; Wu, C.A.; Kang, K. Non-Electrode Components for Rechargeable Aqueous Zinc Batteries: Electrolytes, Solid-Electrolyte-Interphase, Current Collectors, Binders, and Separators. *Adv. Mater.* **2022**, *34*, 2108206. [[CrossRef](#)] [[PubMed](#)]
73. Gao, S.S.; Zhang, Z.; Mao, F.F.; Liu, P.G.; Zhou, Z. Advances and strategies of electrolyte regulation in Zn-ion batteries. *Mater. Chem. Front.* **2023**, *7*, 3232–3258. [[CrossRef](#)]
74. Xu, C.J.; Li, B.H.; Du, H.D.; Kang, F.Y. Energetic Zinc Ion Chemistry: The Rechargeable Zinc Ion Battery. *Angew. Chem.-Int. Ed.* **2012**, *51*, 933–935. [[CrossRef](#)]
75. Zhu, Q.C.; Xiao, Q.; Zhang, B.W.; Yan, Z.C.; Liu, X.; Chen, S.; Ren, Z.F.; Yu, Y. VS<sub>4</sub> with a chain crystal structure used as an intercalation cathode for aqueous Zn-ion batteries. *J. Mater. Chem. A* **2020**, *8*, 10761–10766. [[CrossRef](#)]
76. Zhang, N.; Dong, Y.; Jia, M.; Bian, X.; Wang, Y.Y.; Qiu, M.D.; Xu, J.Z.; Liu, Y.C.; Jiao, L.F.; Cheng, F.Y. Rechargeable Aqueous Zn-V<sub>2</sub>O<sub>5</sub> Battery with High Energy Density and Long Cycle Life. *ACS Energy Lett.* **2018**, *3*, 1366–1372. [[CrossRef](#)]
77. Jia, Z.J.; Wang, B.G.; Wang, Y. Copper hexacyanoferrate with a well-defined open framework as a positive electrode for aqueous zinc ion batteries. *Mater. Chem. Phys.* **2015**, *149*, 601–606. [[CrossRef](#)]
78. Alfaruqi, M.H.; Gim, J.; Kim, S.; Song, J.; Pham, D.T.; Jo, J.; Xiu, Z.; Mathew, V.; Kim, J. A layered  $\delta$ -MnO<sub>2</sub> nanoflake cathode with high zinc-storage capacities for eco-friendly battery applications. *Electrochem. Commun.* **2015**, *60*, 121–125. [[CrossRef](#)]
79. Zhang, N.; Ji, Y.R.; Wang, J.C.; Wang, P.F.; Zhu, Y.R.; Yi, T.F. Understanding of the charge storage mechanism of MnO<sub>2</sub>-based aqueous zinc-ion batteries: Reaction processes and regulation strategies. *J. Energy Chem.* **2023**, *82*, 423–463. [[CrossRef](#)]
80. Tie, Z.W.; Liu, L.J.; Deng, S.Z.; Zhao, D.B.; Niu, Z.Q. Proton Insertion Chemistry of a Zinc-Organic Battery. *Angew. Chem.-Int. Ed.* **2020**, *59*, 4920–4924. [[CrossRef](#)]
81. Liao, Y.X.; Chen, H.C.; Yang, C.; Liu, R.; Peng, Z.W.; Cao, H.J.; Wang, K.K. Unveiling performance evolution mechanisms of MnO<sub>2</sub> polymorphs for durable aqueous zinc-ion batteries. *Energy Storage Mater.* **2022**, *44*, 508–516. [[CrossRef](#)]
82. Sun, W.; Wang, F.; Hou, S.Y.; Yang, C.Y.; Fan, X.L.; Ma, Z.H.; Gao, T.; Han, F.D.; Hu, R.Z.; Zhu, M.; et al. Zn/MnO<sub>2</sub> Battery Chemistry with H<sup>+</sup> and Zn<sup>2+</sup> Coinsertion. *J. Am. Chem. Soc.* **2017**, *139*, 9775–9778. [[CrossRef](#)]
83. Li, L.Y.; Hoang, T.K.A.; Zhi, J.; Han, M.; Li, S.K.; Chen, P. Functioning Mechanism of the Secondary Aqueous Zn- $\beta$ -MnO<sub>2</sub> Battery. *ACS Appl. Mater. Interfaces* **2020**, *12*, 12834–12846. [[CrossRef](#)] [[PubMed](#)]
84. Zhu, K.Y.; Wu, T.; Sun, S.C.; van den Bergh, W.; Stefik, M.; Huang, K. Synergistic H<sup>+</sup>/Zn<sup>2+</sup> dual ion insertion mechanism in high-capacity and ultra-stable hydrated VO<sub>2</sub> cathode for aqueous Zn-ion batteries. *Energy Storage Mater.* **2020**, *29*, 60–70. [[CrossRef](#)]
85. Tian, Y.P.; Ju, M.M.; Bin, X.Q.; Luo, Y.J.; Que, W.X. Long cycle life aqueous rechargeable battery Zn/Vanadium hexacyanoferrate with H<sup>+</sup>/Zn<sup>2+</sup> coinsertion for high capacity. *Chem. Eng. J.* **2022**, *430*, 132864. [[CrossRef](#)]
86. Liu, W.B.; Zhang, X.Y.; Huang, Y.F.; Jiang, B.Z.; Chang, Z.W.; Xu, C.J.; Kang, F.Y.  $\beta$ -MnO<sub>2</sub> with proton conversion mechanism in rechargeable zinc ion battery. *J. Energy Chem.* **2021**, *56*, 365–373. [[CrossRef](#)]
87. Guo, X.; Zhou, J.; Bai, C.L.; Li, X.K.; Fang, G.Z.; Liang, S.Q. Zn/MnO<sub>2</sub> battery chemistry with dissolution-deposition mechanism. *Mater. Today Energy* **2020**, *16*, 100396. [[CrossRef](#)]
88. Yan, H.H.; Zhang, X.K.; Yang, Z.W.; Xia, M.T.; Xu, C.W.; Liu, Y.W.; Yu, H.X.; Zhang, L.Y.; Shu, J. Insight into the electrolyte strategies for aqueous zinc ion batteries. *Coord. Chem. Rev.* **2022**, *452*, 214297. [[CrossRef](#)]
89. Li, Y.F.; Yuan, J.J.; Qiao, Y.F.; Xu, H.; Zhang, Z.H.; Zhang, W.Y.; He, G.Y.; Chen, H.Q. Recent progress in structural modification of polymer gel electrolytes for use in solid-state zinc-ion batteries. *Dalton Trans.* **2023**, *52*, 11780–11796. [[CrossRef](#)]
90. Hu, F.L.; Li, M.Y.; Gao, G.W.; Fan, H.Q.; Ma, L.T. The Gel-State Electrolytes in Zinc-Ion Batteries. *Batteries* **2022**, *8*, 214. [[CrossRef](#)]
91. Dong, H.B.; Li, J.W.; Guo, J.; Lai, F.L.; Zhao, F.J.; Jiao, Y.D.; Brett, D.J.L.; Liu, T.X.; He, G.J.; Parkin, I.P. Insights on Flexible Zinc-Ion Batteries from Lab Research to Commercialization. *Adv. Mater.* **2021**, *33*, 2007548. [[CrossRef](#)] [[PubMed](#)]
92. Iqbal, N.; Ali, Y.; Lee, S. Debonding Mechanisms at the Particle-Binder Interface in the Li-Ion Battery Electrode. *J. Electrochem. Soc.* **2020**, *167*, 060515. [[CrossRef](#)]
93. Iqbal, N.; Choi, J.; Lee, C.; Ayub, H.M.U.; Kim, J.; Kim, M.; Kim, Y.; Moon, D.; Lee, S. Effects of Diffusion-Induced Nonlinear Local Volume Change on the Structural Stability of NMC Cathode Materials of Lithium-Ion Batteries. *Mathematics* **2022**, *10*, 4697. [[CrossRef](#)]
94. Iqbal, N.; Ali, Y.; Lee, S. Mechanical degradation analysis of a single electrode particle with multiple binder connections: A comparative study. *Int. J. Mech. Sci.* **2020**, *188*, 105943. [[CrossRef](#)]
95. Ali, Y.; Iqbal, N.; Lee, S. Role of SEI layer growth in fracture probability in lithium-ion battery electrodes. *Int. J. Energy Res.* **2021**, *45*, 5293–5308. [[CrossRef](#)]
96. Klemm, D.; Heublein, B.; Fink, H.P.; Bohn, A. Cellulose: Fascinating biopolymer and sustainable raw material. *Angew. Chem.-Int. Ed.* **2005**, *44*, 3358–3393. [[CrossRef](#)] [[PubMed](#)]
97. Zheng, Z.Y.; Yan, S.Y.; Zhang, Y.F.; Zhang, X.P.; Zhou, J.; Ye, J.L.; Zhu, Y.S. An ultrathin natural cellulose based hydrogel membrane for the high-performance quasi-solid-state zinc-ion batteries. *Chem. Eng. J.* **2023**, *475*, 146314. [[CrossRef](#)]
98. Yue, X.; Wang, Q.H.; Ao, K.L.; Shi, J.H.; Zhang, X.Y.; Zhao, H.; Uyanga, K.; Yang, Y.; Daoud, W.A. A novel 3D bacterial cellulose network as cathodic scaffold and hydrogel electrolyte for zinc-ion batteries. *J. Power Sources* **2023**, *557*, 232553. [[CrossRef](#)]

99. Cao, G.H.; Zhao, L.; Ji, X.W.; Peng, Y.Y.; Yu, M.M.; Wang, X.Y.; Li, X.Y.; Ran, F. "Salting out" in Hofmeister Effect Enhancing Mechanical and Electrochemical Performance of Amide-based Hydrogel Electrolytes for Flexible Zinc-Ion Battery. *Small* **2023**, *19*, e2207610. [CrossRef]
100. Xu, L.; Meng, T.T.; Zheng, X.Y.; Li, T.Y.; Brozena, A.H.; Mao, Y.M.; Zhang, Q.; Clifford, B.C.; Rao, J.C.; Hu, L.B. Nanocellulose-Carboxymethylcellulose Electrolyte for Stable, High-Rate Zinc-Ion Batteries. *Adv. Funct. Mater.* **2023**, *33*, 2302098. [CrossRef]
101. Mittal, N.; Ojanguren, A.; Kundu, D.; Lizundia, E.; Niederberger, M. Bottom-Up Design of a Green and Transient Zinc-Ion Battery with Ultralong Lifespan. *Small* **2023**, *19*, e2206249. [CrossRef] [PubMed]
102. Zhang, Q.C.; Li, C.W.; Li, Q.L.; Pan, Z.H.; Sun, J.; Zhou, Z.Y.; He, B.; Man, P.; Xie, L.Y.; Kang, L.X.; et al. Flexible and High-Voltage Coaxial-Fiber Aqueous Rechargeable Zinc-Ion Battery. *Nano Lett.* **2019**, *19*, 4035–4042. [CrossRef]
103. Chen, M.F.; Chen, J.Z.; Zhou, W.J.; Han, X.; Yao, Y.G.; Wong, C.P. Realizing an All-Round Hydrogel Electrolyte toward Environmentally Adaptive Dendrite-Free Aqueous Zn-MnO<sub>2</sub> Batteries. *Adv. Mater.* **2021**, *33*, 2007559. [CrossRef] [PubMed]
104. Rinaudo, M. Chitin and chitosan: Properties and applications. *Prog. Polym. Sci.* **2006**, *31*, 603–632. [CrossRef]
105. Wu, M.L.; Zhang, Y.; Xu, L.; Yang, C.P.; Hong, M.; Cui, M.J.; Clifford, B.C.; He, S.M.; Jing, S.S.; Yao, Y.; et al. A sustainable chitosan-zinc electrolyte for high-rate zinc-metal batteries. *Matter* **2022**, *5*, 3402–3416. [CrossRef]
106. Guo, J.; Wang, Y.J.; Li, S.H.; Meng, Y.S.; Qin, Y.Y.; Jiang, L.T.; Huang, H.; Shen, L.D. Regulating zinc deposition for dendrite-free aqueous zinc-ion batteries: A zincophilic chitosan polyelectrolyte hydrogel modified glass fiber separator. *J. Alloys Compd.* **2023**, *967*, 171708. [CrossRef]
107. Guo, J.; Wang, Y.J.; Li, S.H.; Qin, Y.Y.; Meng, Y.S.; Jiang, L.T.; Huang, H.; Shen, L.D. Chitosan hydrogel polyelectrolyte-modified cotton pad as dendrite-inhibiting separators for stable zinc anodes in aqueous zinc-ion batteries. *J. Power Sources* **2023**, *580*, 233392. [CrossRef]
108. Lu, H.Y.; Hu, J.S.; Wei, X.J.; Zhang, K.Q.; Xiao, X.; Zhao, J.X.; Hu, Q.; Yu, J.; Zhou, G.M.; Xu, B.A. A recyclable biomass electrolyte towards green zinc-ion batteries. *Nat. Commun.* **2023**, *14*, 4435. [CrossRef]
109. Wang, F.F.; Zhang, J.P.; Lu, H.T.; Zhu, H.B.; Chen, Z.H.; Wang, L.; Yu, J.Y.; You, C.H.; Li, W.H.; Song, J.W.; et al. Production of gas-releasing electrolyte-replenishing Ah-scale zinc metal pouch cells with aqueous gel electrolyte. *Nat. Commun.* **2023**, *14*, 4211. [CrossRef]
110. Zhan, H.J.; Chen, Y.Z.; Huang, L.; Yang, C.; Zhong, Y.L.; Wang, L.H.; Jiang, X.L. Synthesis and characterization of reversible thermosensitive methylated chitin and its application in zinc-ion battery thermal runaway. *J. Polym. Sci.* **2023**. [CrossRef]
111. Lee, K.Y.; Mooney, D.J. Alginate: Properties and biomedical applications. *Prog. Polym. Sci.* **2012**, *37*, 106–126. [CrossRef] [PubMed]
112. Tang, Y.; Liu, C.X.; Zhu, H.R.; Xie, X.S.; Gao, J.W.; Deng, C.B.; Han, M.M.; Liang, S.Q.; Zhou, J. Ion-confinement effect enabled by gel electrolyte for highly reversible dendrite-free zinc metal anode. *Energy Storage Mater.* **2020**, *27*, 109–116. [CrossRef]
113. Zheng, Z.Y.; Cao, H.C.; Shi, W.H.; She, C.L.; Zhou, X.L.; Liu, L.L.; Zhu, Y.S. Low-Cost Zinc-Alginate-Based Hydrogel-Polymer Electrolytes for Dendrite-Free Zinc-Ion Batteries with High Performances and Prolonged Lifetimes. *Polymers* **2023**, *15*, 212. [CrossRef] [PubMed]
114. Hong, L.; Wu, X.M.; Liu, Y.S.; Yu, C.Y.; Liu, Y.C.; Sun, K.X.; Shen, C.Y.; Huang, W.; Zhou, Y.F.; Chen, J.S.; et al. Self-Adapting and Self-Healing Hydrogel Interface with Fast Zn<sup>2+</sup> Transport Kinetics for Highly Reversible Zn Anodes. *Adv. Funct. Mater.* **2023**, *33*, 2300952. [CrossRef]
115. Zhang, B.Y.; Qin, L.P.; Fang, Y.; Chai, Y.Z.; Xie, X.S.; Lu, B.A.; Liang, S.Q.; Zhou, J. Tuning Zn<sup>2+</sup> coordination tunnel by hierarchical gel electrolyte for dendrite-free zinc anode. *Sci. Bull.* **2022**, *67*, 955–962. [CrossRef] [PubMed]
116. Wang, J.W.; Huang, Y.; Liu, B.B.; Li, Z.X.; Zhang, J.Y.; Yang, G.S.; Hiralal, P.; Jin, S.Y.; Zhou, H. Flexible and anti-freezing zinc-ion batteries using a guar-gum/sodium-alginate/ethylene-glycol hydrogel electrolyte. *Energy Storage Mater.* **2021**, *41*, 599–605. [CrossRef]
117. Fernández-Benito, A.; Martínez-López, J.C.; Jafari, M.J.; Solin, N.; Martínez, J.G.; García-Giménez, D.; Ederth, T.; Inganaes, O.; Carretero-González, J. Green and Scalable Biopolymer-Based Aqueous Polyelectrolyte Complexes for Zinc-Ion Charge Storage Devices. *ChemElectroChem* **2023**, *10*, e202300327. [CrossRef]
118. Karim, A.A.; Bhat, R. Fish gelatin: Properties, challenges, and prospects as an alternative to mammalian gelatins. *Food Hydrocoll.* **2009**, *23*, 563–576. [CrossRef]
119. Su, K.; Wang, C.M. Recent advances in the use of gelatin in biomedical research. *Biotechnol. Lett.* **2015**, *37*, 2139–2145. [CrossRef]
120. Han, Q.; Chi, X.W.; Liu, Y.Z.; Wang, L.; Du, Y.X.; Ren, Y.; Liu, Y. An inorganic salt reinforced Zn<sup>2+</sup>-conducting solid-state electrolyte for ultra-stable Zn metal batteries. *J. Mater. Chem. A* **2019**, *7*, 22287–22295. [CrossRef]
121. García-Ochoa, F.; Santos, V.E.; Casas, J.A.; Gómez, E. Xanthan gum: Production, recovery, and properties. *Biotechnol. Adv.* **2000**, *18*, 549–579. [CrossRef]
122. Mudgil, D.; Barak, S.; Khatkar, B.S. Guar gum: Processing, properties and food applications—A Review. *J. Food Sci. Technol.-Mysore* **2014**, *51*, 409–418. [CrossRef] [PubMed]
123. Ali, B.H.; Ziada, A.; Blunden, G. Biological effects of gum arabic: A review of some recent research. *Food Chem. Toxicol.* **2009**, *47*, 1–8. [CrossRef] [PubMed]
124. Zhang, S.L.; Yu, N.S.; Zeng, S.; Zhou, S.S.; Chen, M.H.; Di, J.T.; Li, Q.W. An adaptive and stable bio-electrolyte for rechargeable Zn-ion batteries. *J. Mater. Chem. A* **2018**, *6*, 12237–12243. [CrossRef]
125. Wang, Y.; Chen, Y.H. A flexible zinc-ion battery based on the optimized concentrated hydrogel electrolyte for enhanced performance at subzero temperature. *Electrochim. Acta* **2021**, *395*, 139178. [CrossRef]

126. Huang, Y.; Zhang, J.Y.; Liu, J.W.; Li, Z.X.; Jin, S.Y.; Li, Z.G.; Zhang, S.D.; Zhou, H. Flexible and stable quasi-solid-state zinc ion battery with conductive guar gum electrolyte. *Mater. Today Energy* **2019**, *14*, 100349. [[CrossRef](#)]
127. Wu, K.; Cui, J.; Yi, J.; Liu, X.Y.; Ning, F.H.; Liu, Y.Y.; Zhang, J.J. Biodegradable Gel Electrolyte Suppressing Water-Induced Issues for Long-Life Zinc Metal Anodes. *ACS Appl. Mater. Interfaces* **2022**, *14*, 34612–34619. [[CrossRef](#)]
128. Xu, W.W.; Liu, C.Z.; Wu, Q.L.; Xie, W.W.; Kim, W.Y.; Lee, S.Y.; Gwon, J. A stretchable solid-state zinc ion battery based on a cellulose nanofiber-polyacrylamide hydrogel electrolyte and a  $\text{Mg}_{0.23}\text{V}_2\text{O}_5 \cdot 1.0\text{H}_2\text{O}$  cathode. *J. Mater. Chem. A* **2020**, *8*, 18327–18337. [[CrossRef](#)]
129. Li, Z.L.; Zhou, G.Q.; Ye, L.; He, J.Y.; Xu, W.W.; Hong, S.; Chen, W.M.; Li, M.C.; Liu, C.Z.; Mei, C.T. High-energy and dendrite-free solid-state zinc metal battery enabled by a dual-network and water-confinement hydrogel electrolyte. *Chem. Eng. J.* **2023**, *472*, 144992. [[CrossRef](#)]
130. Mao, Y.C.; Ren, H.Z.; Zhang, J.C.; Luo, T.; Liu, N.N.; Wang, B.; Le, S.R.; Zhang, N.Q. Modifying hydrogel electrolyte to induce zinc deposition for dendrite-free zinc metal anode. *Electrochim. Acta* **2021**, *393*, 139094. [[CrossRef](#)]
131. Zhang, H.D.; Gan, X.T.; Song, Z.P.; Zhou, J.P. Amphoteric Cellulose-Based Double-Network Hydrogel Electrolyte Toward Ultra-Stable Zn Anode. *Angew. Chem.-Int. Ed.* **2023**, *62*, e202217833. [[CrossRef](#)]
132. Gomez, I.; Alesanco, Y.; Blazquez, J.A.; Viñuales, A.; Colmenares, L.C. Room-Temperature Self-Standing Cellulose-Based Hydrogel Electrolytes for Electrochemical Devices. *Polymers* **2020**, *12*, 2686. [[CrossRef](#)] [[PubMed](#)]
133. Jia, C.E.; Zhang, X.S.; Liang, S.J.; Fu, Y.C.; Liu, W.T.; Chen, J.Z.; Liu, X.Y.; Zhang, L.L. Environmentally adaptable hydrogel electrolyte with the triple interpenetrating network in the flexible zinc-ion battery with ultralong stability. *J. Power Sources* **2022**, *548*, 232072. [[CrossRef](#)]
134. Lin, P.X.; Cong, J.L.; Li, J.Y.; Zhang, M.H.; Lai, P.B.; Zeng, J.; Yang, Y.; Zhao, J.B. Achieving ultra-long lifespan Zn metal anodes by manipulating desolvation effect and Zn deposition orientation in a multiple cross-linked hydrogel electrolyte. *Energy Storage Mater.* **2022**, *49*, 172–180. [[CrossRef](#)]
135. Xu, W.W.; Liu, C.Z.; Ren, S.X.; Lee, D.; Gwon, J.; Flake, J.C.; Lei, T.Z.; Baisakh, N.; Wu, Q.L. A cellulose nanofiber-polyacrylamide hydrogel based on a co-electrolyte system for solid-state zinc ion batteries to operate at extremely cold temperatures. *J. Mater. Chem. A* **2021**, *9*, 25651–25662. [[CrossRef](#)]
136. Wu, T.; Zhou, W.J.; Quan, Y.H.; Chen, M.F.; Tian, Q.H.; Han, X.; Xu, J.L.; Chen, J.Z. Facile and green synthesis of nanocellulose with the assistance of ultraviolet light irradiation for high-performance quasi-solid-state zinc-ion batteries. *J. Colloid Interfaces Sci.* **2022**, *628*, 1–9. [[CrossRef](#)]
137. Liu, Q.J.; Ji, Z.Y.; Mo, F.N.; Ling, W.; Wang, J.Q.; Lei, H.; Cui, M.W.; Zhang, Z.S.; Liu, Y.; Cheng, L.K.; et al. Stable Thermochromic Hydrogel for a Flexible and Wearable Zinc-Ion Yarn Battery with High-Temperature Warning Function. *ACS Appl. Energy Mater.* **2022**, *5*, 12448–12455. [[CrossRef](#)]
138. Li, Y.Q.; Miao, R.T.; Yang, Y.; Han, L.; Han, Q.S. A zinc-ion battery-type self-powered strain sensing system by using a high-performance ionic hydrogel. *Soft Matter* **2023**, *19*, 8022–8032. [[CrossRef](#)]
139. Liu, C.Z.; Xu, W.W.; Mei, C.T.; Li, M.C.; Chen, W.M.; Hong, S.; Kim, W.Y.; Lee, S.Y.; Wu, Q.L. A Chemically Self-Charging Flexible Solid-State Zinc-Ion Battery Based on  $\text{VO}_2$  Cathode and Polyacrylamide-Chitin Nanofiber Hydrogel Electrolyte. *Adv. Energy Mater.* **2021**, *11*, 2003902. [[CrossRef](#)]
140. Li, Y.Q.; Yang, Y.; Liu, X.H.; Yang, Y.W.; Wu, Y.Y.; Han, L.; Han, Q.S. Flexible self-powered integrated sensing system based on a rechargeable zinc-ion battery by using a multifunctional polyacrylamide/carboxymethyl chitosan/LiCl ionic hydrogel. *Colloids Surf. A-Physicochem. Eng. Asp.* **2022**, *648*, 129254. [[CrossRef](#)]
141. Dong, H.B.; Li, J.W.; Zhao, S.Y.; Jiao, Y.D.; Chen, J.T.; Tan, Y.S.; Brett, D.J.L.; He, G.J.; Parkin, I.P. Investigation of a Biomass Hydrogel Electrolyte Naturally Stabilizing Cathodes for Zinc-Ion Batteries. *ACS Appl. Mater. Interfaces* **2021**, *13*, 745–754. [[CrossRef](#)]
142. Qiu, M.H.; Liu, H.Q.; Tawiah, B.; Jia, H.; Fu, S.H. Zwitterionic triple-network hydrogel electrolyte for advanced flexible zinc ion batteries. *Compos. Commun.* **2021**, *28*, 100942. [[CrossRef](#)]
143. Wang, B.J.; Li, J.M.; Hou, C.Y.; Zhang, Q.H.; Li, Y.G.; Wang, H.Z. Stable Hydrogel Electrolytes for Flexible and Submarine-Use Zn-Ion Batteries. *ACS Appl. Mater. Interfaces* **2020**, *12*, 46005–46014. [[CrossRef](#)] [[PubMed](#)]
144. Mostafavi, F.S.; Zaeim, D. Agar-based edible films for food packaging applications—A review. *Int. J. Biol. Macromol.* **2020**, *159*, 1165–1176. [[CrossRef](#)]
145. Zarrintaj, P.; Manouchehri, S.; Ahmadi, Z.; Saeb, M.R.; Urbanska, A.M.; Kaplan, D.L.; Mozafari, M. Agarose-based biomaterials for tissue engineering. *Carbohydr. Polym.* **2018**, *187*, 66–84. [[CrossRef](#)] [[PubMed](#)]
146. Zheng, Z.Y.; Shi, W.H.; Zhou, X.L.; Zhang, X.P.; Guo, W.L.; Shi, X.Y.; Xiong, Y.; Zhu, Y.S. Agar-based hydrogel polymer electrolyte for high-performance zinc-ion batteries at all climatic temperatures. *Iscience* **2023**, *26*, 106437. [[CrossRef](#)]
147. Jiang, D.; Lu, N.; Li, L.B.; Zhang, H.Q.; Luan, J.S.; Wang, G.B. A highly compressible hydrogel electrolyte for flexible Zn-MnO<sub>2</sub> battery. *J. Colloid Interfaces Sci.* **2022**, *608*, 1619–1626. [[CrossRef](#)]
148. Cao, Y.P.; Mezzenga, R. Design principles of food gels. *Nat. Food* **2020**, *1*, 106–118. [[CrossRef](#)]
149. Zhou, J.; Li, Y.; Xie, L.; Xu, R.; Zhang, R.; Gao, M.; Tian, W.; Li, D.; Qiao, L.; Wang, T.; et al. Humidity-sensitive, shape-controllable, and transient zinc-ion batteries based on plasticizing gelatin-silk protein electrolytes. *Mater. Today Energy* **2021**, *21*, 100712. [[CrossRef](#)]

150. Shi, G.; Peng, X.W.; Zeng, J.M.; Zhong, L.X.; Sun, Y.; Yang, W.; Zhong, Y.L.; Zhu, Y.X.; Zou, R.; Admassie, S.; et al. A Liquid Metal Microdroplets Initialized Hemicellulose Composite for 3D Printing Anode Host in Zn-Ion Battery. *Adv. Mater.* **2023**, *35*, e2300109. [[CrossRef](#)]
151. Lu, Y.Y.; Wang, Z.H.; Li, M.; Li, Z.Y.; Hu, X.Y.; Xu, Q.J.; Wang, Y.H.; Liu, H.M.; Wang, Y.G. 3D Printed Flexible Zinc Ion Micro-Batteries with High Areal Capacity toward Practical Application. *Adv. Funct. Mater.* **2023**, 2310966. [[CrossRef](#)]

**Disclaimer/Publisher's Note:** The statements, opinions and data contained in all publications are solely those of the individual author(s) and contributor(s) and not of MDPI and/or the editor(s). MDPI and/or the editor(s) disclaim responsibility for any injury to people or property resulting from any ideas, methods, instructions or products referred to in the content.